Supporting Information

Heteromultivalency enables enhanced detection of nucleic acid mutations

Brendan R. Deal, Rong Ma, Hiroaki Ogasawara, James T. Kindt, and Khalid Salaita

Department of Chemistry, Emory University, Atlanta, Georgia 30322, United States

Table of Contents

1. Materials

1.1. Oligonucleotide Sequences and Modifications

All oligonucleotides were custom synthesized by Integrated DNA Technologies (Coralville, IA). The table below includes the names and sequences for all oligonucleotides used in this work. The structures of each of the oligonucleotide modifications are also included below.

Name	Sequence (5' to 3')
7S	/5ThioMC6-D/TTTTTTTTTTACAAGCT
8S	/5ThioMC6-D/TTTTTTTTTTCACAAGCT
9S	/5ThioMC6-D/TTTTTTTTTTCCACAAGCT
10S	/5ThioMC6-D/TTTTTTTTTTGCCACAAGCT
11S	/5ThioMC6-D/TTTTTTTTTTCGCCACAAGCT
4T	/5ThioMC6-D/TTTTTTTTTTCCAA
5T	/5ThioMC6-D/TTTTTTTTTTCCAAC
6T	/5ThioMC6-D/TTTTTTTTTTCCAACT
7T	/5ThioMC6-D/TTTTTTTTTTCCAACTA
8T	/5ThioMC6-D/TTTTTTTTTTCCAACTAC
9T	/5ThioMC6-D/TTTTTTTTTTCCAACTACC
10T	/5ThioMC6-D/TTTTTTTTTTCCAACTACCA
no spacer G12C	TGGTAGTTGGAGCTTGTGGCGTAGG/3AmMO/
no spacer WT	TGGTAGTTGGAGCTGGTGGCGTAGG/3AmMO/
internal short spacer G12C	TGGTAGTTGG/iSp9/AGCTTGTGGCGTAGG/3AmMO/
internal short spacer WT	TGGTAGTTGG/iSp9/AGCTGGTGGCGTAGG/3AmMO/
internal long spacer G12C	TGGTAGTTGG/iSp18/AGCTTGTGGCGTAGG/3AmMO/
internal long spacer WT	TGGTAGTTGG/iSp18/AGCTGGTGGCGTAGG/3AmMO/
terminal short spacer G12C	/5Sp9/TGGTAGTTGGAGCTTGTGGCGTAGG/3AmMO/
terminal short spacer WT	/5Sp9/TGGTAGTTGGAGCTGGTGGCGTAGG/3AmMO/
terminal long spacer G12C	/5Sp18/TGGTAGTTGGAGCTTGTGGCGTAGG/3AmMO/
terminal long spacer WT	/5Sp18/TGGTAGTTGGAGCTGGTGGCGTAGG/3AmMO/
3' thiol 8T	CCAACTACTTTTTTTTTT/3ThioMC3-D/
3' thiol 8S	CACAAGCTTTTTTTTTTT/3ThioMC3-D/
3' thiol 9S	CCACAAGCTTTTTTTTTTT/3ThioMC3-D/
5' thiol 8S L19F	/5ThioMC6-D/TTTTTTTTTTCGTGAAGG
5' thiol 9S L19F	/5ThioMC6-D/TTTTTTTTTTCGTGAAGGC
G12C/L19F	AGCTTGTGGCGTAGGCAAGAGTGCCTTCACG/3AmMO/
WT/L19F	AGCTGGTGGCGTAGGCAAGAGTGCCTTCACG/3AmMO/
G12C/WT	AGCTTGTGGCGTAGGCAAGAGTGCCTTGACG/3AmMO/
WT/WT	AGCTGGTGGCGTAGGCAAGAGTGCCTTGACG/3AmMO/
8S Q498R	GGTCGGAATTTTTTTTTT/3ThioMC3-D/
9S Q498R	GGGTCGGAATTTTTTTTTT/3ThioMC3-D/
8S Y505H	/5ThioMC6-D/TTTTTTTTTTTGGTGACC
9S Y505H	/5ThioMC6-D/TTTTTTTTTTTGGTGACCA
complement to Omicron target	/5ThioMC6D/TTTTTTTTTTTGGTGACCAACACCATAAGTGGGTCGGAA
Q498R/N501Y/Y505H target (Omicron)	TTCCGACCCACTTATGGTGTTGGTCACCA/3AmMO/
WT/WT/WT target (Original)	TTCCAACCCACTAATGGTGTTGGTTACCA/3AmMO/
WT/N501Y/WT target (Alpha)	TTCCAACCCACTTATGGTGTTGGTTACCA/3AmMO/

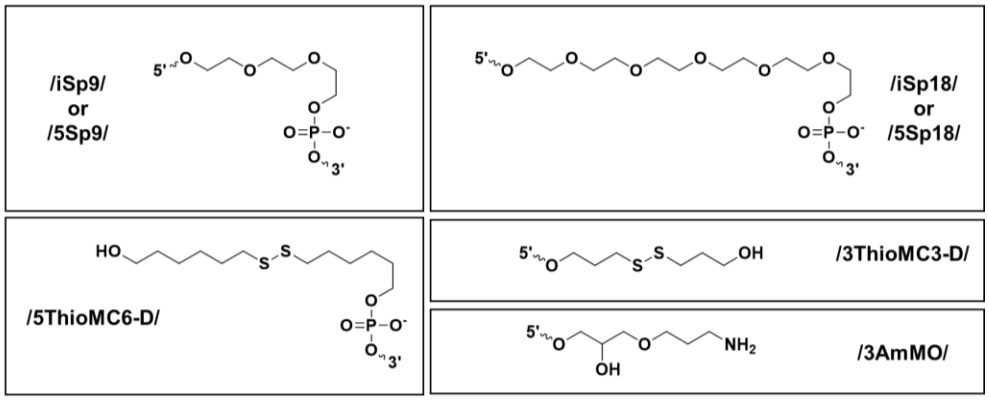

1.2. Reagents

5 µm aminated silica beads (Cat# SA06N) were purchased from Bangs Laboratory (Fishers, IN). Dri-solv methylsulfoxide (Cat# MX1457-7) was purchased from EMD Millipore (Burlington, MA). Potassium hydroxide (Cat# 221473), sodium bicarbonate (Cat#S6014), acetonitrile (Cat# 34998), and Atto647N NHS ester (Cat#18373-1MG-F) were purchased from Sigma-Aldrich (St. Louis, MO). 20x TE buffer (Cat# 42020325-2) was purchased from bioWORLD (Dublin, OH). Bond-Breaker TCEP (Tris(2-carboxyethyl)phosphine hydrochloride) solution, Neutral pH (Cat#77720), Quant-IT Oligreen ssDNA reagent (Cat# O7582), SMCC (succinimidyl 4-(N-maleimidomethyl)cyclohexane-1-carboxylate) (Cat#22360), sulfo-NHS-acetate (Cat#26777), and Tween20 (Cat# BP337) were purchased from Thermo Fisher Scientific (Waltham, MA). Saline sodium citrate (SSC) buffer (Cat# AM9763) was purchased from Ambion (Austin, TX). Triethylammonium acetate (Cat# 60-4110-57) was purchased from Glen Research (Sterling, VA).

1.3. Consumables

96-well white flat bottom polystyrene microplates (Cat# 3912) were purchased from Corning (Corning, NY). P2 size exclusion gel (Cat#1504118) and P4 size exclusion gel (Cat# #1504124) was purchased from Bio-Rad (Hercules, CA). Nanosep MF centrifugal devices (Cat# ODM02C35) were purchased from Pall Laboratory.

2. Equipment

The major equipment that was used in this study includes: CytoFLEX flow cytometer (Beckman coulter), Nanodrop 2000 UV-Vis Spectrophotometer (Thermo Scientific), Barnstead nanopure water purifying system (Thermo Fisher), 5424 R centrifuge (Eppendorf), Synergy H1 plate reader (Biotek), high-performance liquid chromatography 1100 (Agilent) with AdvanceBio Oligonucleotide C18 column (653950-702, 4.6x 150 mm, 2.7 µm) (Agilent), LTQ Orbitrap Velos mass spectrometer (Thermo Scientific), Galaxy mini tabletop centrifuge (VWR), Rebel Brightfield Microscope (ECHO), and Nikon Ti2-E motorized research microscope equipped with SOLA SE II 365 Light Engine, Photometrics Prime 95B-25mm Back-illuminated sCMOS camera, and CF-L AT Cy5/Alexa 647/Draq 5 filter set.

3. Methods

Modeling. In all modeling calculations herein, c_{eff} = 50 uM, MM = 0.025, and the ratio of consecutive values for K_{eq} chosen = 20. These values were chosen to most closely reproduce experimental results obtained.

To derive an equation to calculate the equilibrium binding occupancy, Θ, of the oligos coating the particle surface using the total binding affinity of the target (K_{eq}), total target

concentration ($[target]$), and total concentration of oligos on the particle surface ($[surface]$) we began with the standard equation for K_{eq} :

$$K_{eq} = \frac{[surface_{bound}]}{[target_{unbound}][surface_{unbound}]}$$

This equation is then rearranged into the following form:

$$K_{eq}[target_{unbound}] = \frac{[surface_{bound}]}{[surface_{unbound}]}$$

$[surface_{bound}]$ is then replaced with $[surface_{total}] - [surface_{unbound}]$ to give the following equation:

$$K_{eq}[target_{unbound}] = \frac{[surface_{total}] - [surface_{unbound}]}{[surface_{unbound}]}$$

As $[surface_{total}] - [surface_{unbound}] = \Theta$ and $[surface_{unbound}] = 1 - \Theta$, the following equation is then derived.

$$\frac{\Theta}{1 - \Theta} = K_{eq}[target_{unbound}]$$

In order to solve for Θ using only K_{eq}, $[target]$, and $[surface]$, $[target_{unbound}]$ is first replaced with $[target] - [target_{bound}]$:

$$\frac{\Theta}{1 - \Theta} = K_{eq}([target] - [target_{bound}])$$

$[target_{bound}]$ is replaced with $[surface]\Theta$ to give the following equation:

$$\frac{\Theta}{1 - \Theta} = K_{eq}([target] - [surface]\Theta)$$

This equation is then rearranged into a quadratic form ($\Theta = a\Theta^2 + b\Theta + c$) as follows:

$$\Theta = (1 - \Theta)(K_{eq}([target] - K_{eq}[surface]\Theta)$$

$$\Theta = K_{eq}[surface]\Theta^2 - K_{eq}[target]\Theta - K_{eq}[surface]\Theta + K_{eq}[target]$$

$$0 = K_{eq}[surface]\Theta^2 - K_{eq}[target]\Theta - K_{eq}[surface]\Theta - \Theta + K_{eq}[target]$$

$$0 = K_{eq}[surface]\Theta^2 + (-K_{eq}([target] - [surface]) - 1)\Theta + K_{eq}[target]$$

The equation is then solved for Θ using the quadratic formula:

$$\Theta = \frac{-b \pm \sqrt{b^2 - 4ac}}{2a}$$

Where $a = K_{eq}[surface]$, $b = -K_{eq}([target] - [surface]) - 1$, and $c = K_{eq}[target]$, giving the final equation for Θ:

$$\Theta = \frac{K_{eq}([target] + [surface]) + 1 \pm \sqrt{(K_{eq}([target] + [surface]) + 1)^2 - 4{K_{eq}}^2[surface][target]}}{2K_{eq}[surface]}$$

where the correct value of Θ is equal to the root given by subtracting the quadratic portion. For the results shown in Figure 1D, E, and G, $[target]$ = 1 nM and $[surface]$ = 1 nM, and thus the following simplifications can be made:

$$\Theta = \frac{2K_{eq} + 1 \pm \sqrt{(2K_{eq} + 1)^2 - 4{K_{eq}}^2}}{2K_{eq}}$$

$$\Theta = \frac{1}{2K_{eq}} + 1 \pm \frac{\sqrt{4{K_{eq}}^2 + 4K_{eq} + 1 - 4{K_{eq}}^2}}{2K_{eq}}$$

$$\Theta = \frac{1}{2K_{eq}} + 1 \pm \frac{\sqrt{4K_{eq} + 1}}{2K_{eq}}$$

For the results shown in Figure 1F, $[target_1]$ = 0.5 nM and $[target_2]$ = 0.5 nM. Therefore, values of Θ for $target_1$ and for $target_2$ are calculated and then summed to calculate total Θ. Finally, Θ was converted to an arbitrary assay signal, *I*, using the equation:

$$I = I_{max} * + I_{bg}$$

where I_{max} represents the maximum signal and I_{bg} is the background signal when target concentration = 0. In all modeling calculations herein, I_{max} = 250000 and I_{bg} = 58.

The 10 possible sequence pairs when considering two mutations (SNP_1 and SNP_2) on two gene copies ($target_1$ and $target_2$) are as follows:

1. $target_1$ = SNP_1/SNP_2 and $target_2$ = SNP_1/SNP_2 (homozygous double, SNP_1 and SNP_2)
2. $target_1$ = SNP_1/SNP_2 and $target_2$ = SNP_1/WT_2
3. $target_1$ = SNP_1/SNP_2 and $target_2$ = WT_1/SNP_2
4. $target_1$ = SNP_1/SNP_2 and $target_2$ = WT_1/WT_2 (heterozygous cis)
5. $target_1$ = SNP_1/WT_2 and $target_2$ = SNP_1/WT_2 (homozygous single, SNP_1)
6. $target_1$ = SNP_1/WT_2 and $target_2$ = WT_1/SNP_2 (heterozygous trans)
7. $target_1$ = SNP_1/WT_2 and $target_2$ = WT_1/WT_2
8. $target_1$ = WT_1/SNP_2 and $target_2$ = WT_1/SNP_2 (homozygous single, SNP_2)
9. $target_1$ = WT_1/SNP_2 and $target_2$ = WT_1/WT_2
10. $target_1$ = WT_1/WT_2 and $target_2$ = WT_1/WT_2 (wildtype)

The equations for total binding affinity to the SNP_1/SNP_2, SNP_1/WT_2, WT_1/SNP_2, and WT_1/WT_2 targets can be described as:

$$\text{Total } K_{eq,SNP1/SNP2} = K_{eq,S1} + K_{eq,S2} + K_{eq,S1} * K_{eq,S2} * c_{eff}$$

$$\text{Total } K_{eq,SNP1/WT2} = K_{eq,S1} + MM_2 * K_{eq,S2} + K_{eq,S1} * MM_2 * K_{eq,S2} * c_{eff}$$

$$\text{Total } K_{eq,WT1/SNP2} = MM_1 * K_{eq,S1} + K_{eq,S2} + MM_1 * K_{eq,S1} * K_{eq,S2} * c_{eff}$$

$$\text{Total } K_{eq,WT1/WT2} = MM_1 * K_{eq,S1} + MM_2 * K_{eq,S2} + MM_1 * K_{eq,S1} * MM_2 * K_{eq,S2} * c_{eff}$$

where MM_1 corresponds to a mismatch in S_1' and MM_2 corresponds to a mismatch in S_2'.

Synthesis of DNA-functionalized silica particles. 5 µm amine-modified silica particles were suspended in DMSO at a concentration of ~4.4 x 10^5 particles/µL. A 100 mg/mL stock of SMCC was then prepared in DMSO and added at a final concentration of 10 mg/mL to a solution of 4 x 10^4 particles/µL suspended in DMSO. The reaction was then incubated at room temperature for 30 min to prepare maleimide-labeled silica beads. During the reaction of SMCC with the amine-modified silica beads, 0.5 µL of 100 µM thiolated DNA (1 µM final), 0.5 µL of 10 mM TCEP (100 µM final), and 49 µL of 1x PBS at pH 6.8 were mixed and incubated at room temperature for 30 min to 1 hour to reduce the thiolated DNA. The maleimide-labeled silica bead solution was then centrifuged on a tabletop mini-centrifuge at 6000 rpm for 1 min and the supernatant was removed and replaced with an equal volume of a 1 mg/mL solution of sulfo-NHS acetate dissolved in DMSO. The reaction was then incubated at room temperature for 30 min to prepare passivated, maleimide-labeled silica beads. Following the 30 min incubation, centrifugation and supernatant removal was performed 4 times. After each of the first three centrifugations, the beads were resuspended in a 2x volume of DMSO. Following the third resuspension, the beads were split into 50 µL aliquots and then centrifuged for the 4th time. After the 4th centrifugation, the supernatant was removed and replaced with the 50 µL solution of 1 µM reduced thiol-DNA and incubated at room temperature overnight or > 8 hours. For *n*=2 beads, a pre-mixed solution containing 500 nM of each oligo was added, resulting in a total concentration of 1 µM of DNA. Following incubation, 50 µL of 1x SSC, 0.1% Tween20 was added to each tube to help with centrifugation. Next, centrifugation and supernatant removal was performed 4 times. After each of the first three centrifugations, the beads were resuspended in 100 µL of 1x SSC, 0.1% Tween20. After the fourth centrifugation, the beads were resuspended in 1 mL of 1x SSC, 0.1% Tween20.

Determining number of oligos per silica particle. The approximate concentration of the DNA-coated bead stocks was approximated using four representative stock solutions using a hemacytometer. Then, two volumes containing ~1 x 10^5 or ~1.75 x 10^5 beads were taken from the four different DNA-coated bead stocks. Centrifugation at 6000 rpm with the tabletop mini-centrifuge and supernatant removal were then performed for each sample, followed by resuspension of the beads in 100 µL of 0.1 M KOH. The beads were incubated in the KOH solution at room temperature for > 8 hours. Brightfield microscopy images before and after KOH incubation were obtained using the Rebel Brightfield Microscope (Echo). The bead solution was then centrifuged again, and the supernatant was removed in added to a new tube. The centrifuged bead solution was resuspended in 1x SSC, 0.1% Tween20 and analyzed using flow cytometry to confirm that the beads were etched/dissolved fully. The tube containing the removed supernatant was then filtered using P2 gel filtration to remove KOH from the solution. 20x TE buffer was then added to the solution to give a final 1x concentration of TE buffer. Samples were then transferred to a 96 well plate. Oligreen was then added to the solution at a final concentration of 1x and incubated for ~5 min at room temperature before the fluorescence was measured using the Biotek plate reader. To generate a standard curve of fluorescence vs. [DNA], 0, 5, 10, 20, 35, and 50 nM solutions of unreduced thiol DNA were prepared and incubated in a solution of 0.1 M KOH for > 1 hour. Following KOH incubation, the DNA solution was filtered using P2 gel filtration to remove KOH from the solution. 20x TE buffer was then added to the solution to give a final 1x concentration of TE buffer. Samples were then transferred to a 96 well plate. Oligreen was then added to the solution at a final concentration of 1x and incubated for ~5 min at room temperature before the fluorescence was measured using the Biotek plate reader. Using the standard curve, the concentration of DNA in the bead samples was determined and then divided by initial bead concentration to determine the number of oligos per silica bead.

Atto647N conjugation to target strands. Excess NHS-Atto647N (250 µg) was dissolved in 10 µL of fresh DMSO and then added to 10 nmol of amine-labeled target strands in 1x PBS with 0.1 M NaHCO3. The reaction was left for > 1 hour at room temperature. After incubation, unreacted NHS-Atto647N and salts were removed by P2 or P4 gel filtration and purified using an analytical-scale reverse-phase HPLC with an Agilent AdvanceBio Oligonucleotide C18 column. Product was eluted in Solvents A: 0.1 M TEAA and B: ACN with a linear gradient of 10-100% Solvent B over 45 min at 0.5 mL/min flow rate. The molecular weight of the products was evaluated with an electron spray ionization (ESI) method using a Thermo Fisher Scientific Orbitrap. The samples were prepared in a mixture of 70% nanopure water and 30% methanol containing 10 µM ethylenediaminetetraacetic acid (EDTA), 0.0375% triethylamine, and 0.75% of 1,1,1,3,3,3-hexafluoro-2-propanol (HFIP) and the spectra were recorded with negative charge mode eluted with the same solution.[1] The main peak of the obtained ESI-MS spectrum (*m/z*) was then deconvoluted to obtain the average molecular weight for the oligonucleotides. The concentration of the strands was determined by UV-Vis using a Nanodrop instrument.

Flow cytometry assay and analysis to measure target binding. 1 nM Atto647N-labeled target was added to ~2.5 x 10^4 DNA-coated silica beads suspended in 1x SSC, 0.1% Tween20 and incubated at room temperature for 1 hour. Following the 1 hour incubation, centrifugation at 6000 rpm with the tabletop mini-centrifuge and supernatant removal was performed 4 times. After each of the four centrifugations, the beads were resuspended in 100 µL of 1x SSC, 0.1% Tween20. Fully washed beads were then injected into the flow cytometer for final analysis. After performing flow cytometry, FlowJo V10 was used to analyze the data. Singlet beads were isolated from the sample by gating first using forward scatter and side scatter area and second using forward and side scatter height. The median fluorescence intensity of the singlet beads from each sample was then calculated.

Fluorescence microscopy of Atto647N-labeled targets hybridized to beads. Wells in a glass bottom 96-well plate were soaked in ethanol for 5 min, rinsed with Nanopure water, and coated in 10% BSA for 15 min and rinsed again prior to imaging. 0 or 1 nM Atto647N-labeled target was added to ~2.5 x 10^4 DNA-coated silica beads suspended in 1x SSC, 0.1% Tween20 and incubated at room temperature for >1 hour. Following the incubation, centrifugation at 6000 rpm with the tabletop mini-centrifuge and supernatant removal was performed 4 times. After each of the four centrifugations, the beads were resuspended in 100 µL of 1x SSC, 0.1% Tween20. Fully washed beads were then added to the 96-well microscopy plate and imaged on the fluorescence microscope. Brightfield images were obtained and Atto647N images were acquired using a Cy5 cube. Images were processed using Fiji ImageJ software.

Figure S1. Modeling the specificity of homoMV particles for single mutant targets.
(A) Scheme showing binding pathway of a homoMV particle binding either a SNP-containing target or a WT target and modification of binding affinity equation with MM factor. (B) Predicted arbitrary signals when a homoMV particle with different affinities binds the SNP target or the WT target. (C) Predicted discrimination factors for a homoMV particle with different affinities. Red dots correspond to discrimination factors for six values of K_{eq} chosen to mimic a series of oligos of length x, $x + 1$, … , $x + 5$ nt. The black dashed curve was generated by fitting the predicted values to a gaussian distribution in GraphPad.

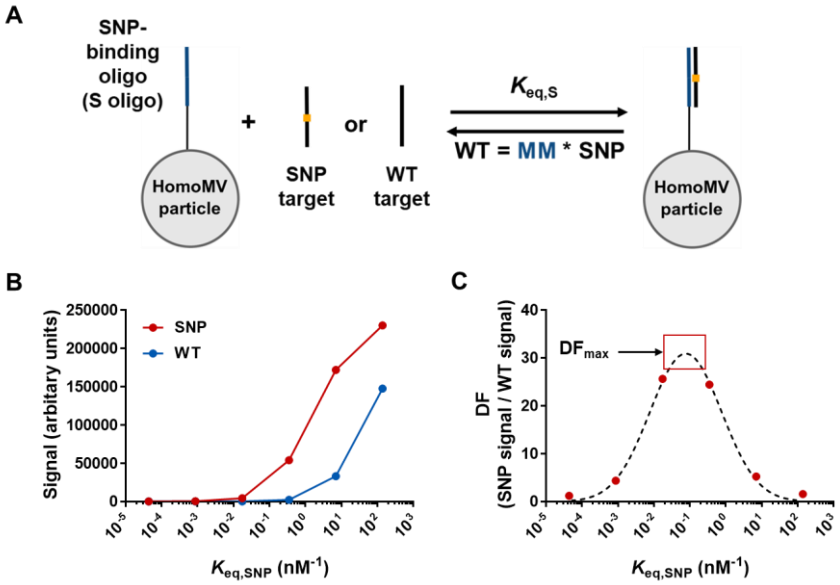

Figure S2. Modeling the specificity of heteroMV particles for single mutant targets.
(A) Scheme showing the two-step reversible binding pathway of an *n*=2 heteroMV particle binding either a SNP-containing target or a WT target and corresponding equations used to model the binding affinity to each target. (B and C) Heatmap showing the predicted arbitrary signals when binding the SNP target (B) or WT target (C) as the monovalent binding affinities of the S and the T oligo are varied. (D) Predicted discrimination factors for an *n*=2 heteroMV particle as the affinity of T ($K_{eq,T\ only}$) is increased (different colors) causing the total affinity for the SNP target ($K_{eq,S+T,SNP}$) to increase (x-axis) for each discrete value of $K_{eq,S\ only}$ chosen (same color dots). The curves were generated by fitting the predicted values to a gaussian distribution in GraphPad. (E) The maximum DF value predicted from the curve in (D) for each discrete value of $K_{eq,T\ only}$. (F) Heatmap showing the predicted discrimination factor when the monovalent binding affinities of the S and the T oligo are varied. Black boxes indicate the *n*=1 and *n*=2 combination with the highest discrimination factors. (G) Heatmap showing the predicted cooperativity factor when the monovalent binding affinities of the S and the T oligo are varied. Black box indicates the *n*=2 combination with the highest cooperativity factor.

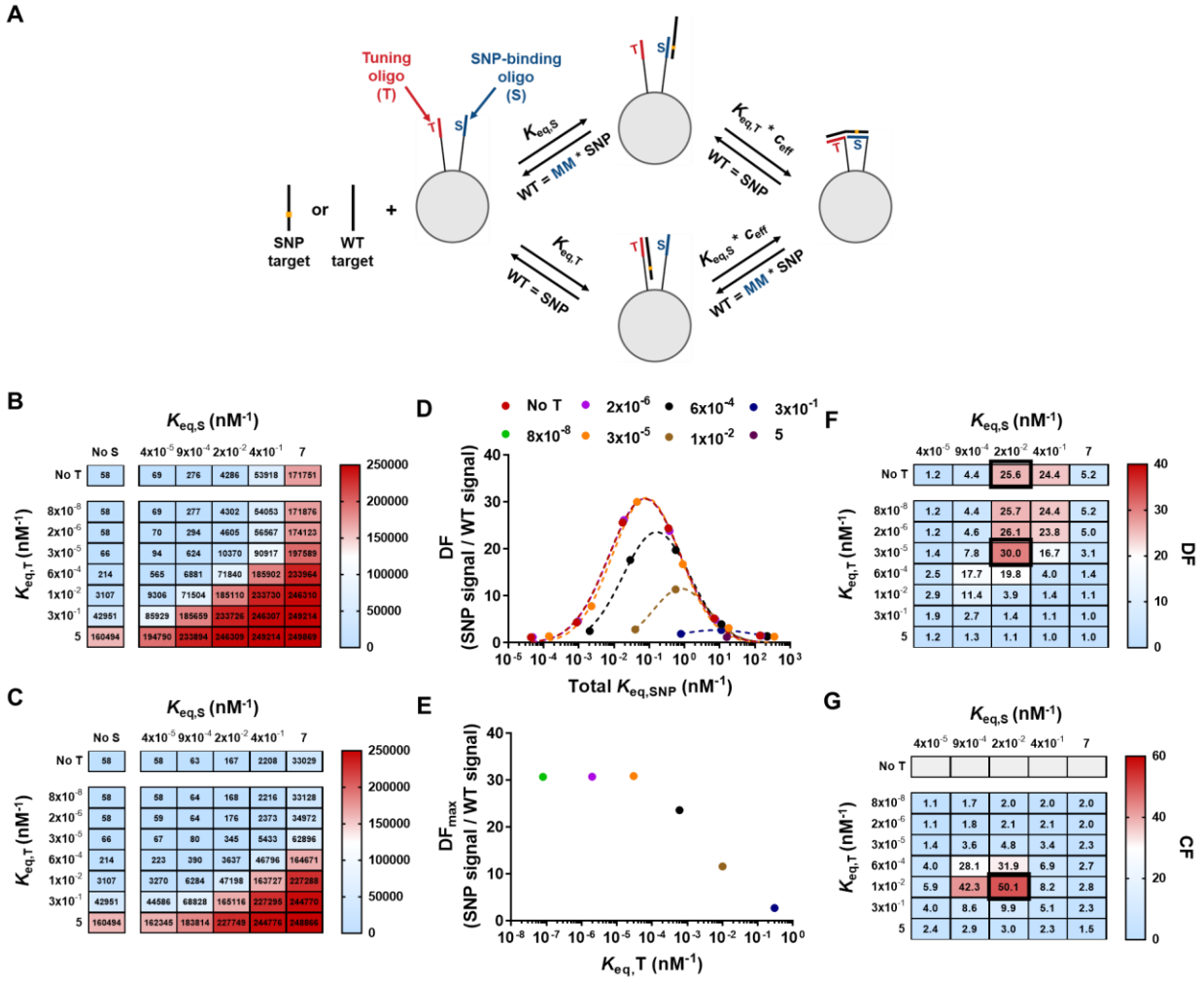

Figure S3. Modeling the specificity of heteroMV particles for double mutant targets.
(A) Scheme showing the two-step reversible binding pathway of an *n*=2 heteroMV particle binding either a double mutant target or a double WT target and corresponding equations used to model the binding affinity to each target. (B) Heatmap showing the predicted cis/trans discrimination factor when the monovalent binding affinities of the S_1 and the S_2 oligo are varied. Black box indicates the *n*=2 combination with the highest predicted cis/trans discrimination factor. (C) Heatmap showing the predicted double mutant discrimination factor when the monovalent binding affinities of the S_1 and the S_2 oligo are varied. Black box indicates the *n*=2 combination with the highest predicted double mutant discrimination factor.

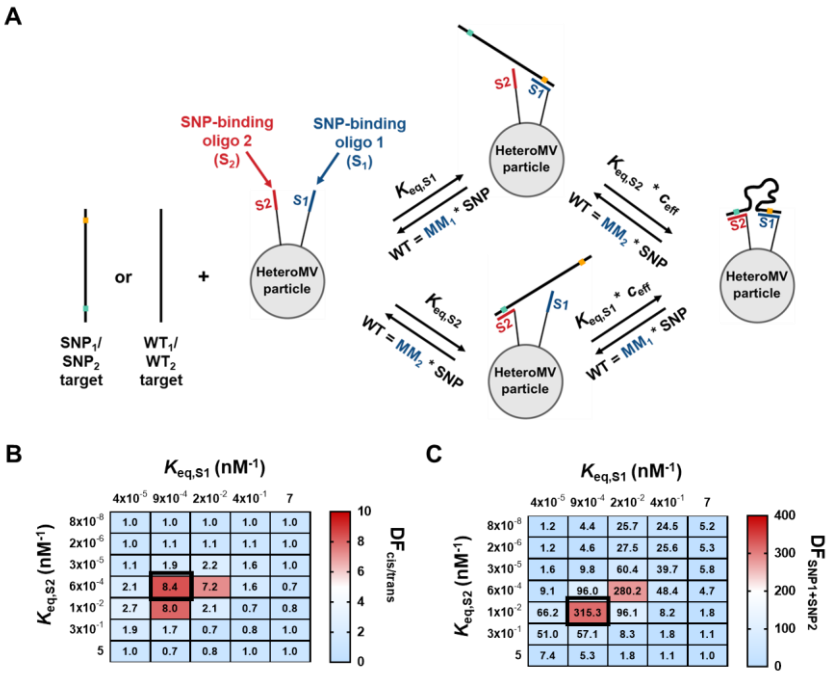

Figure S4. Description of targets and NUPACK predictions of target secondary structure. (A) Scheme describing the DNA sequence (NCBI Reference Sequence: NG_007524.2) and amino acid sequence (NCBI Reference Sequence: NP_001356715.1) of the first 20 amino acids of human KRAS protein. The location of the no spacer targets used in this work are shown in red, with the G12C mutated codon shown in blue. (B and C) Predictions for the secondary structures of the no spacer G12C (B) and WT (C) targets generated using NUPACK. In the illustration on the left, the circle color of each nucleotide refers to the identity of each nucleobase. In the illustration on the right, the circle color of each nucleotide refers to the probability that each nucleotide is bound at equilibrium if it is shown bound or unbound if it is shown unbound. The black arrows refer to the position of the G12C mutation in the target sequence. (D) The location of the G12C/L19F targets used in this work are shown in red, with the G12C and L19F mutated codons shown in blue. (E, F, G, and H) Predictions for the secondary structures of the G12C/L19F (E), WT/L19F (F), G12C/WT (G), and WT/WT (H) targets generated using NUPACK. The black arrows refer to the position of the G12C and L19F mutations in the target sequence. (I) Scheme describing the DNA sequence (NCBI Reference Sequence: NC_045512.2) and amino acid sequence (NCBI Reference Sequence: YP_009724390.1) of amino acids 497-506 of SARS-CoV-2 spike protein. The location of the Omicron/Original/Alpha targets used in this work are shown in red, with the Q498R, N501Y, and Y505H mutated codons shown in blue. (J, K, L) Predictions for the secondary structures of the Omicron (J), Original (K), and Alpha (L) targets generated using NUPACK. The black arrows refer to the position of the Q498R, N501Y, and Y505 mutations in the target sequence. All predictions were performed at 0.15 M Na^+, 0 M Mg^{2+}, and 22°C.

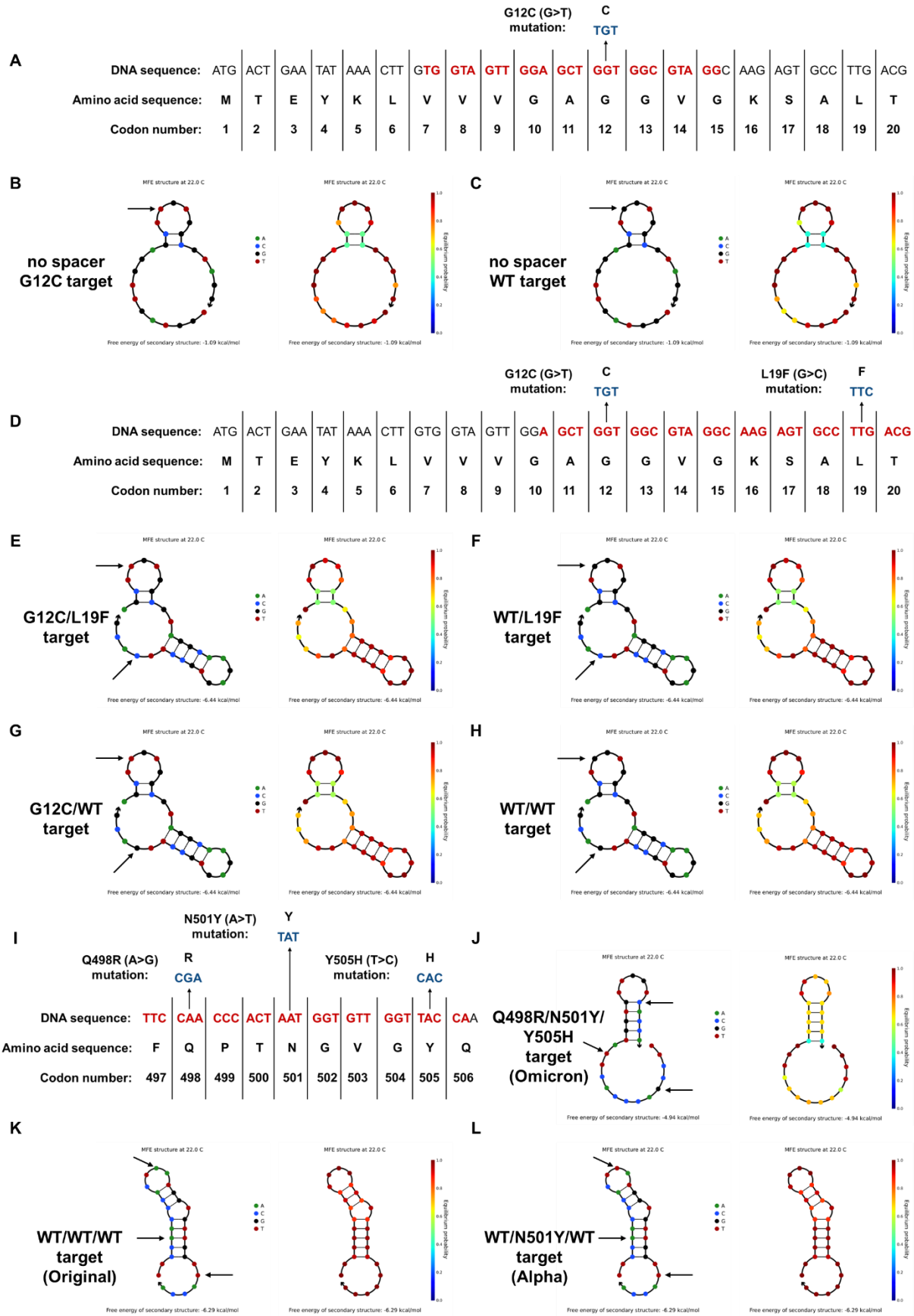
A
G12C (G>T) mutation:
C
TGT
DNA sequence: ATG ACT GAA TAT AAA CTT GTG GTA GTT GGA GCT GGT GGC GTA GGC AAG AGT GCC TTG ACG
Amino acid sequence: M T E Y K L V V V G A G G V G K S A L T
Codon number: 1 2 3 4 5 6 7 8 9 10 11 12 13 14 15 16 17 18 19 20
B
no spacer G12C target
C
no spacer WT target
D
G12C (G>T) mutation:
C
TGT
L19F (G>C) mutation:
F
TTC
DNA sequence: ATG ACT GAA TAT AAA CTT GTG GTA GTT GGA GCT GGT GGC GTA GGC AAG AGT GCC TTG ACG
Amino acid sequence: M T E Y K L V V V G A G G V G K S A L T
Codon number: 1 2 3 4 5 6 7 8 9 10 11 12 13 14 15 16 17 18 19 20
E
G12C/L19F target
F
WT/L19F target
G
G12C/WT target
H
WT/WT target
I
N501Y (A>T) mutation:
Y
TAT
Q498R (A>G) mutation:
R
CGA
Y505H (T>C) mutation:
H
CAC
DNA sequence: TTC CAA CCC ACT AAT GGT GTT GGT TAC CAA
Amino acid sequence: F Q P T N G V G Y Q
Codon number: 497 498 499 500 501 502 503 504 505 506
J
Q498R/N501Y/ Y505H target (Omicron)
K
WT/WT/WT target (Original)
L
WT/N501Y/WT target (Alpha)
MFE structure at 22.0 C
Free energy of secondary structure: -1.09 kcal/mol
Free energy of secondary structure: -6.44 kcal/mol
Free energy of secondary structure: -4.94 kcal/mol
Free energy of secondary structure: -6.29 kcal/mol
Equilibrium probability

Figure S5. Synthesis and purification of Atto647N-labeled targets.
(A) Reaction scheme for conjugation of amine-modified oligonucleotides with NHS-Atto647N. (B) HPLC traces of the Atto647N-labeled targets. Arrows represent the material collected from HPLC.

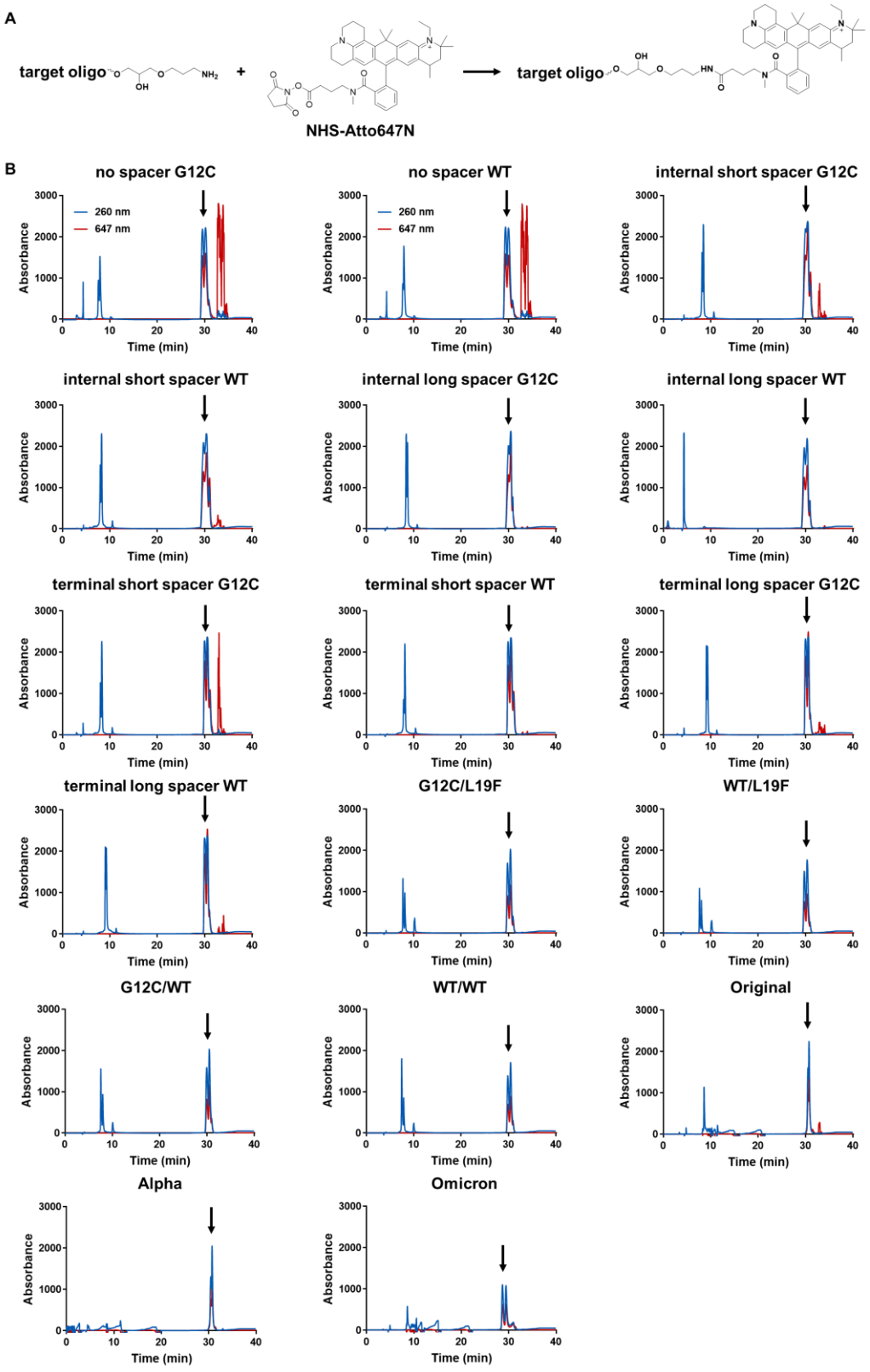

Figure S6. Mass spectrometry characterization of Atto647N-labeled targets.
(A) Table of calculated masses, measured m/z values found, and difference in mass between calculated and measured masses of Atto647N-labeled targets. (B) Raw ESI mass spectra of Atto647N-labeled targets.

A

Sample	Calculated mass (Da)	m/z found (Da)	Difference (Da)
no spacer G12C	8680.17	8679.72	0.45
no spacer WT	8705.27	8704.72	0.55
internal short spacer G12C	8892.37	8891.76	0.61
internal short spacer WT	8917.37	8916.76	0.61
internal long spacer G12C	9024.47	9023.84	0.63
internal long spacer WT	9049.57	9048.84	0.73
terminal short spacer G12C	8892.37	8891.75	0.62
terminal short spacer WT	8917.37	8916.76	0.61
terminal long spacer G12C	9024.47	9023.83	0.64
terminal long spacer WT	9049.57	9048.84	0.73
G12C/L19F	10432.37	10431.01	1.36
WT/L19F	10457.37	10457.02	0.35
G12C/WT	10472.37	10472.02	0.35
WT/WT	10497.37	10497.03	0.34
Original	9667.87	9667.43	0.44
Alpha	9658.87	9658.41	0.46
Omicron	9659.87	9659.41	0.46

B

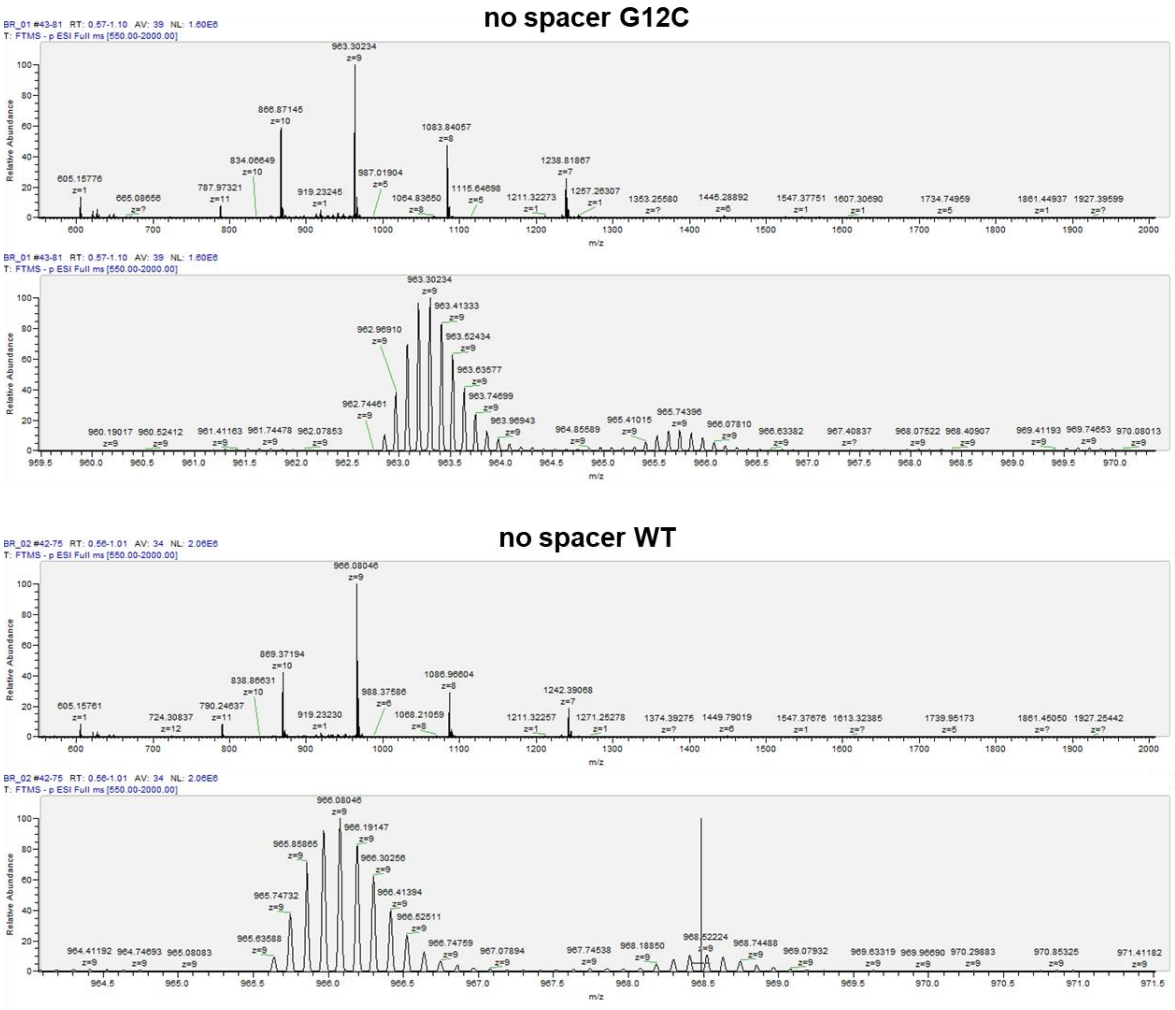

internal short spacer G12C

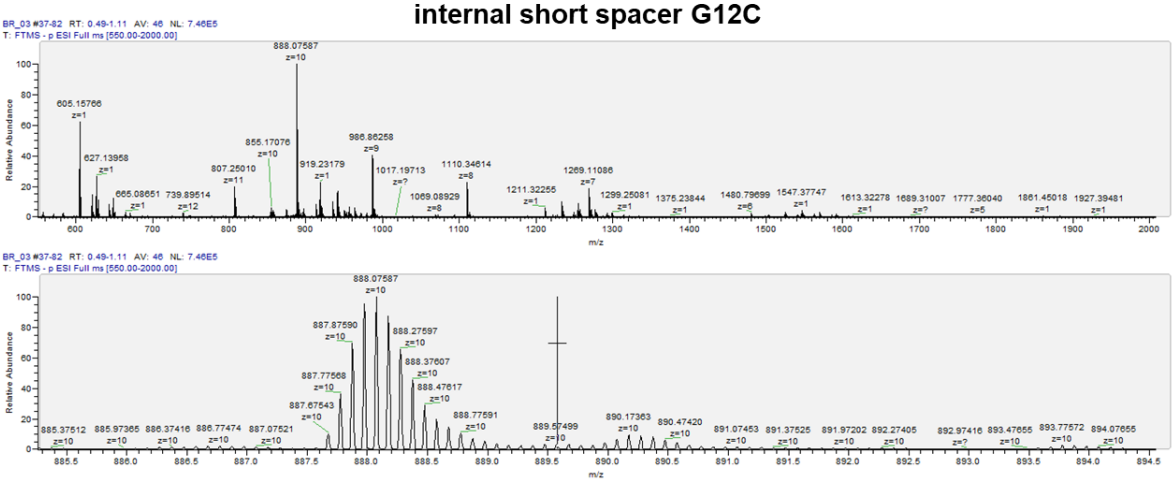

internal short spacer WT

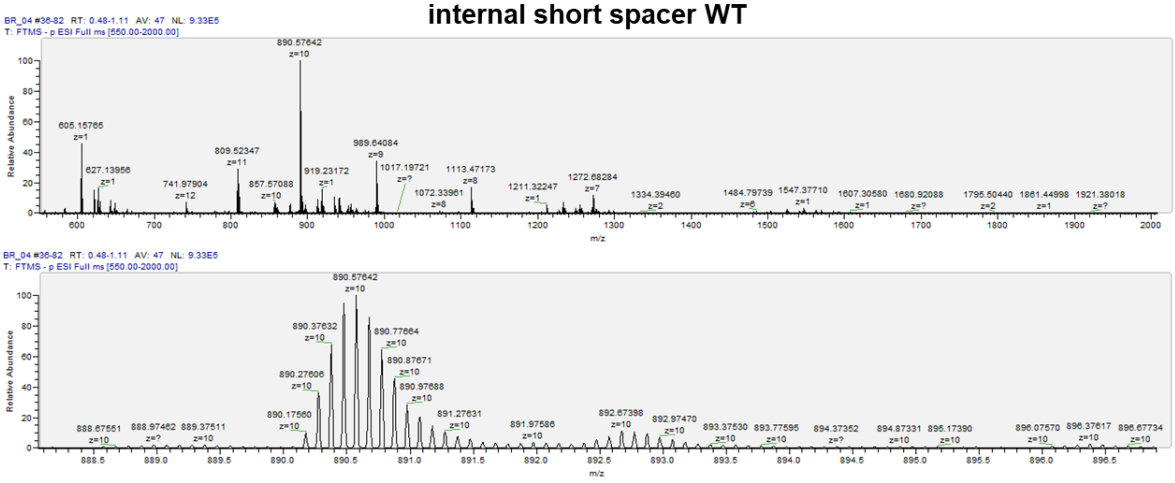

internal long spacer G12C

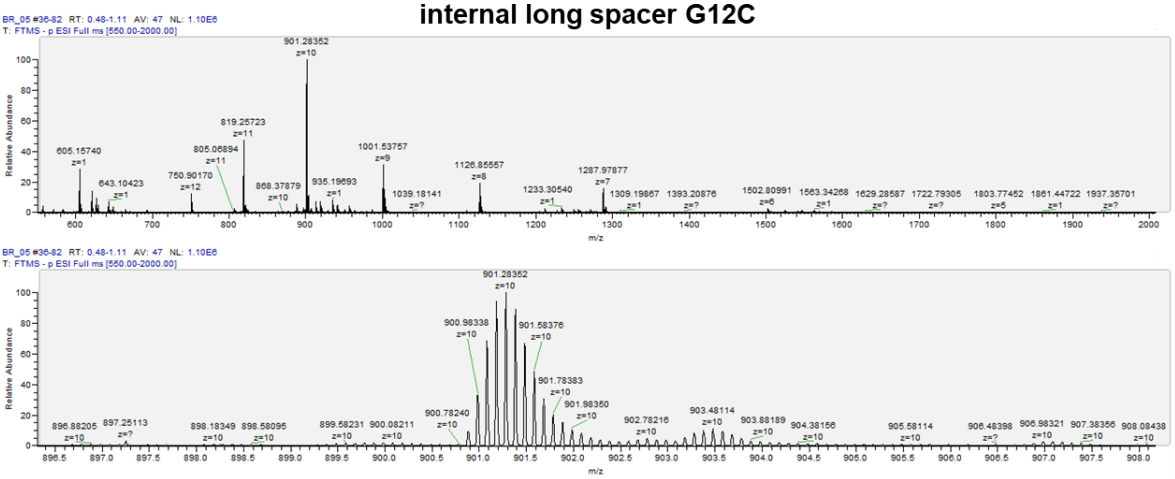

internal long spacer WT

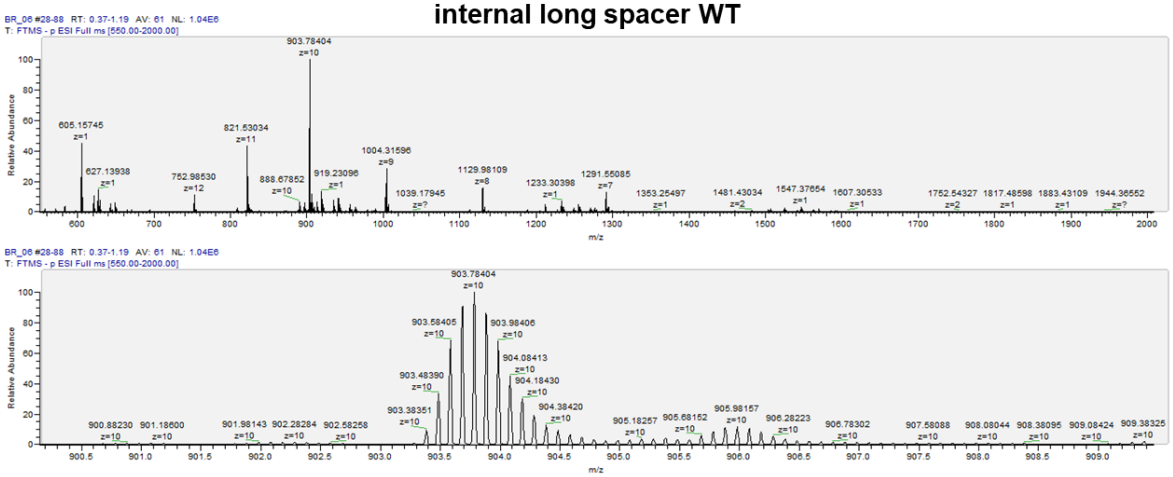

terminal short spacer G12C

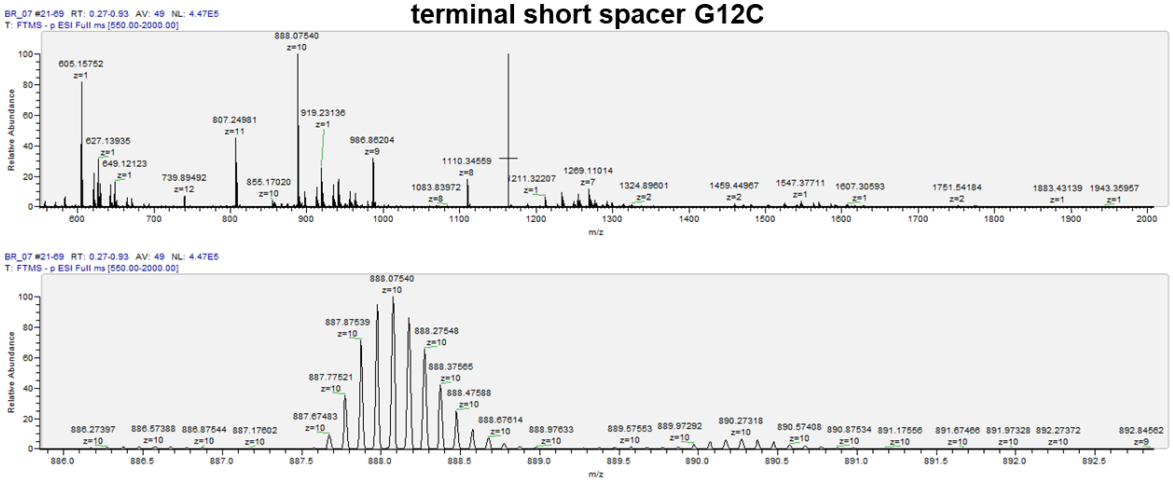

terminal short spacer WT

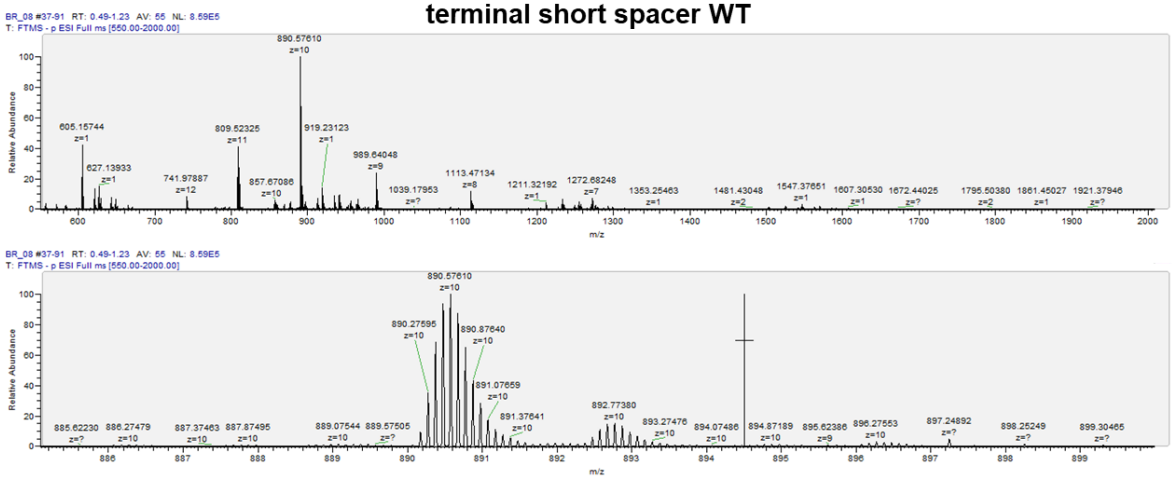

terminal long spacer G12C

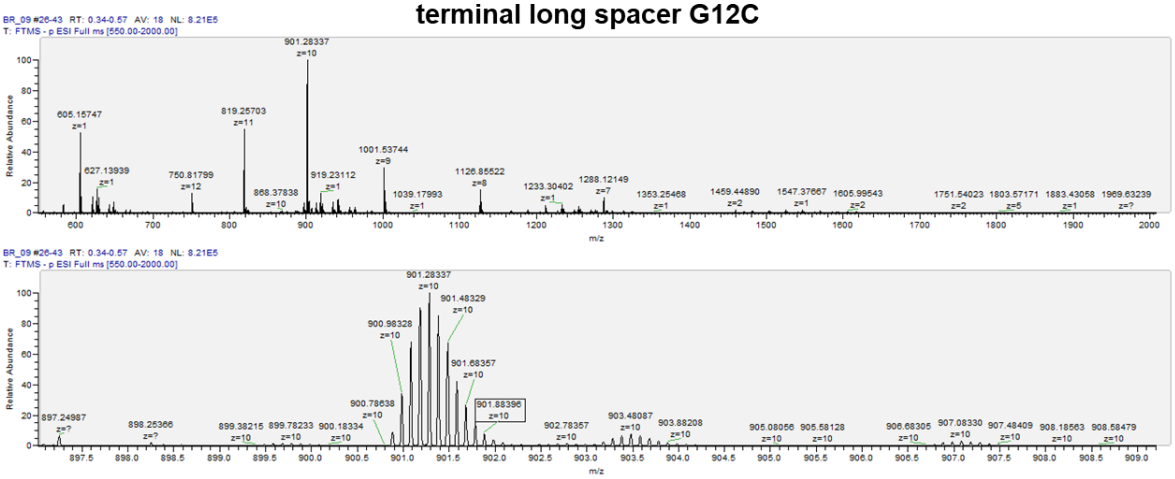

terminal long spacer WT

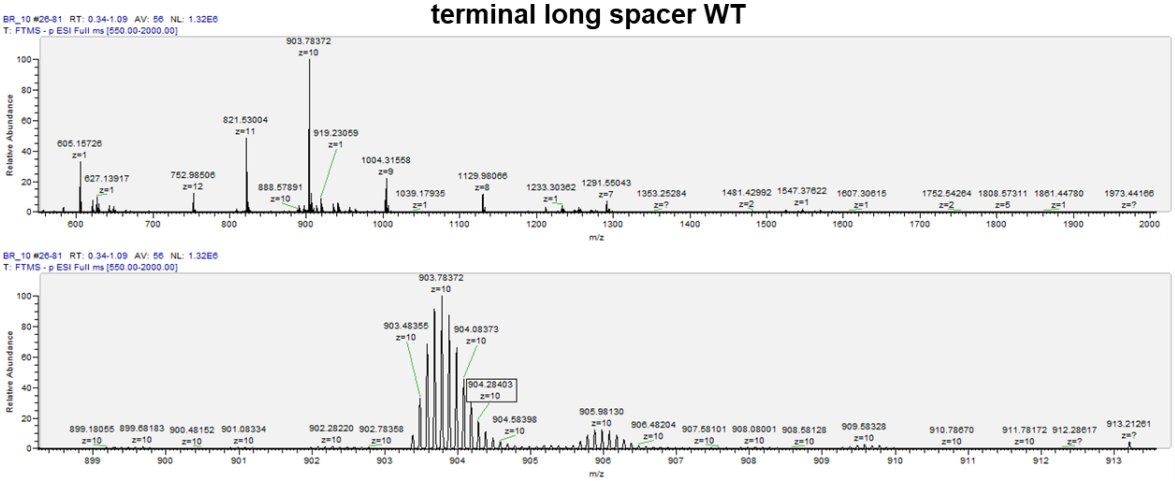

G12C/L19F

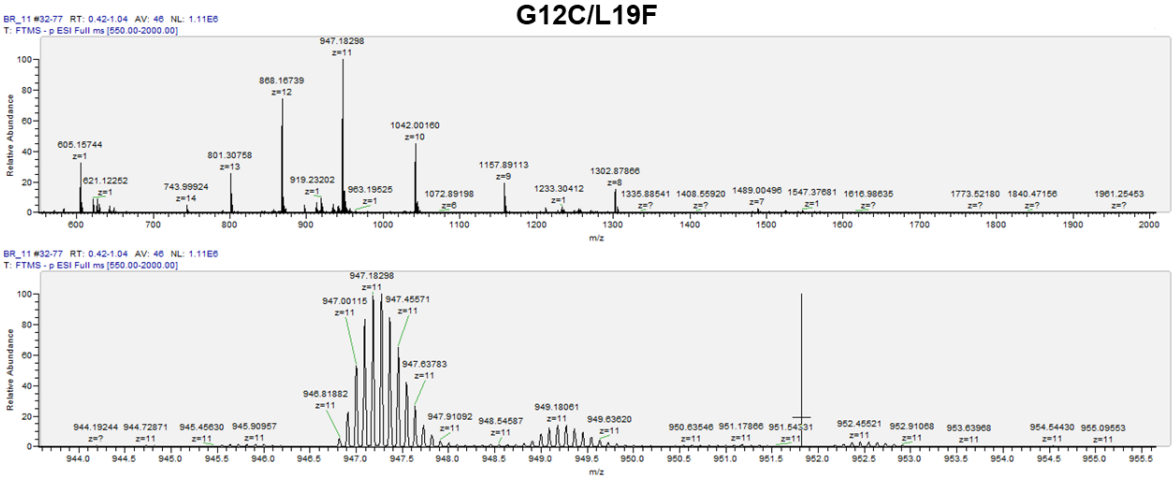

WT/L19F

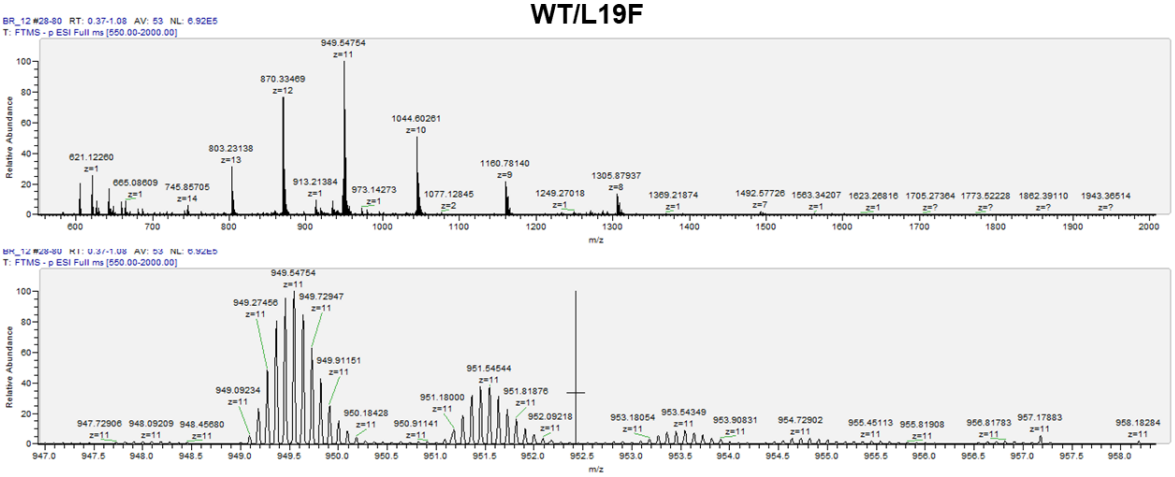

G12C/WT

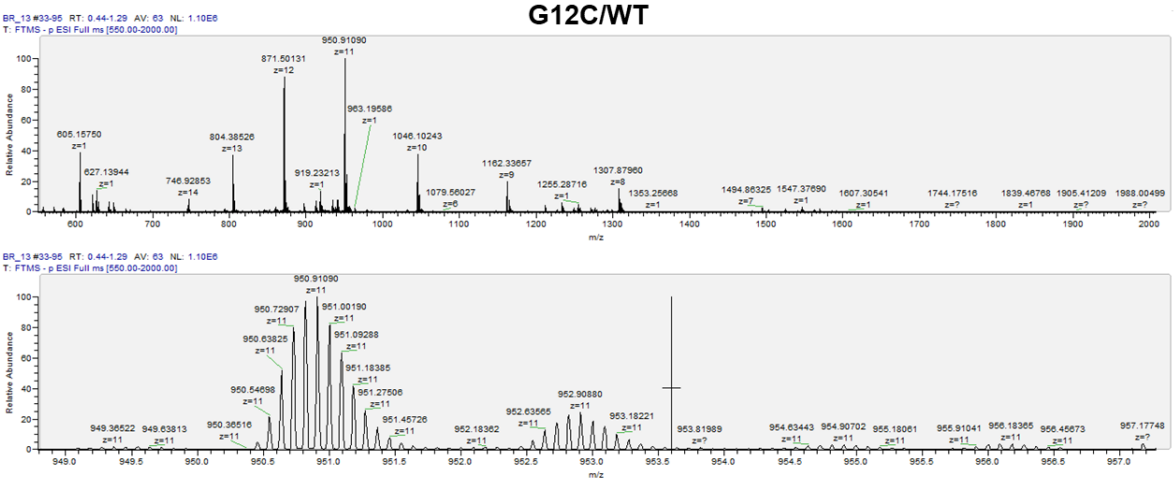

WT/WT

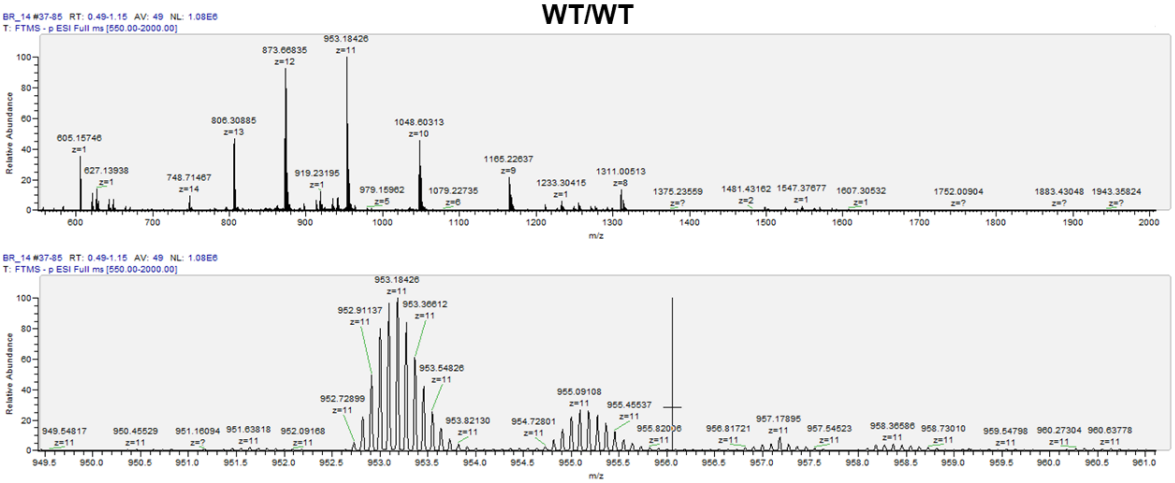

Original

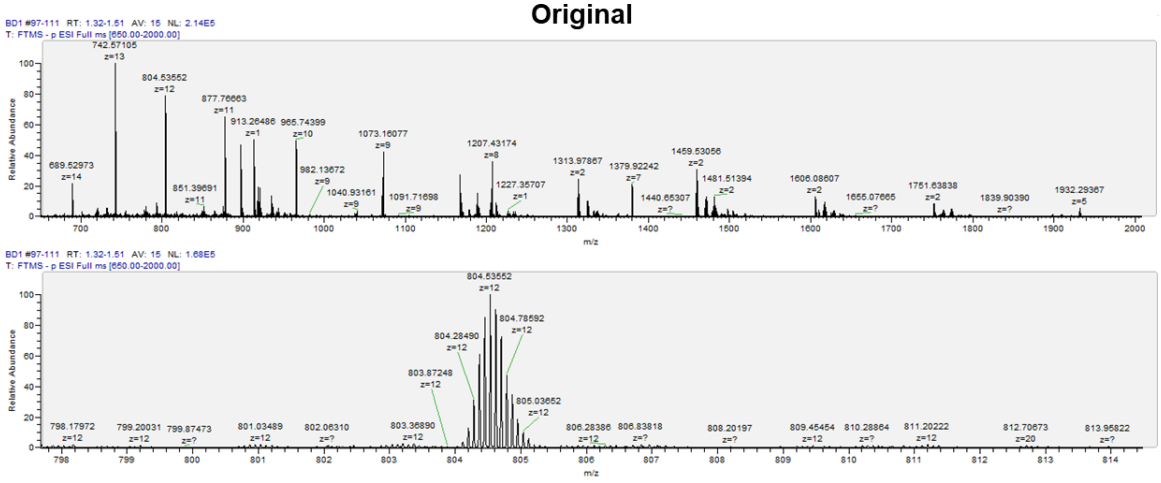

Alpha

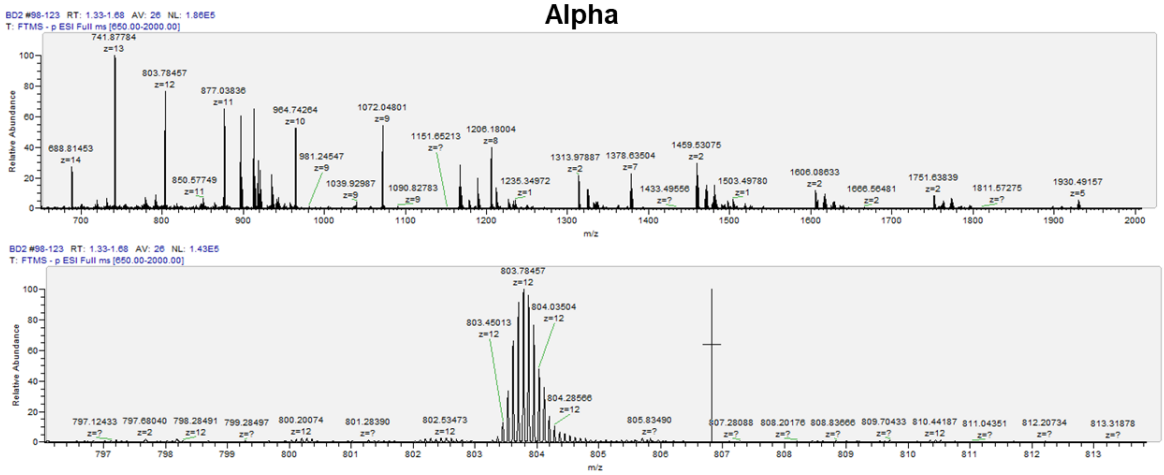

Omicron

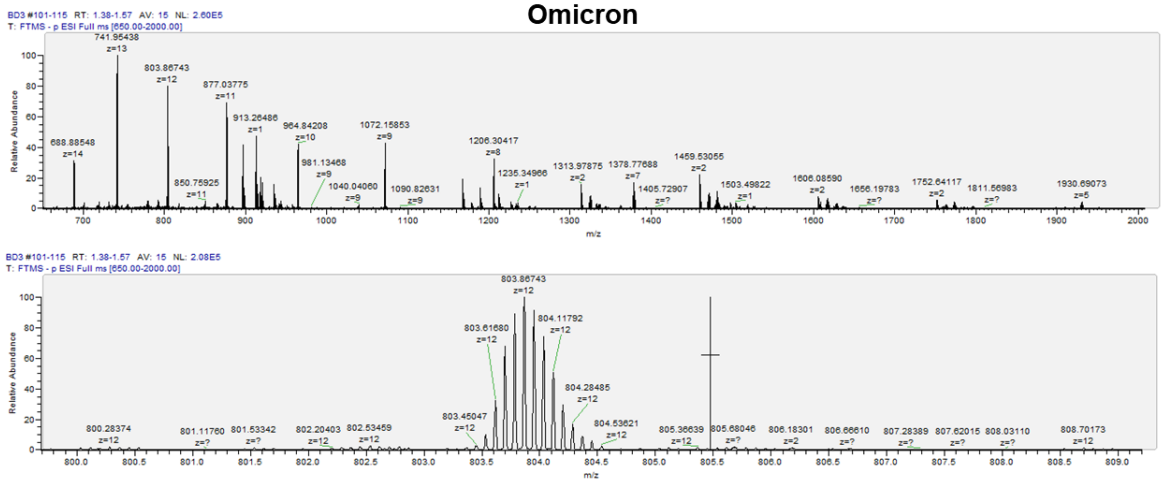

Figure S7. Synthesis of DNA-functionalized silica particles.
Scheme describing the synthesis of DNA-functionalized silica particles. On top is a simplified summary of the synthesis, whereas the boxes on the bottom provide further synthetic details and structures of the reagents used. Refer to methods section “Synthesis of DNA-functionalized silica particles” for a complete description of the synthesis.

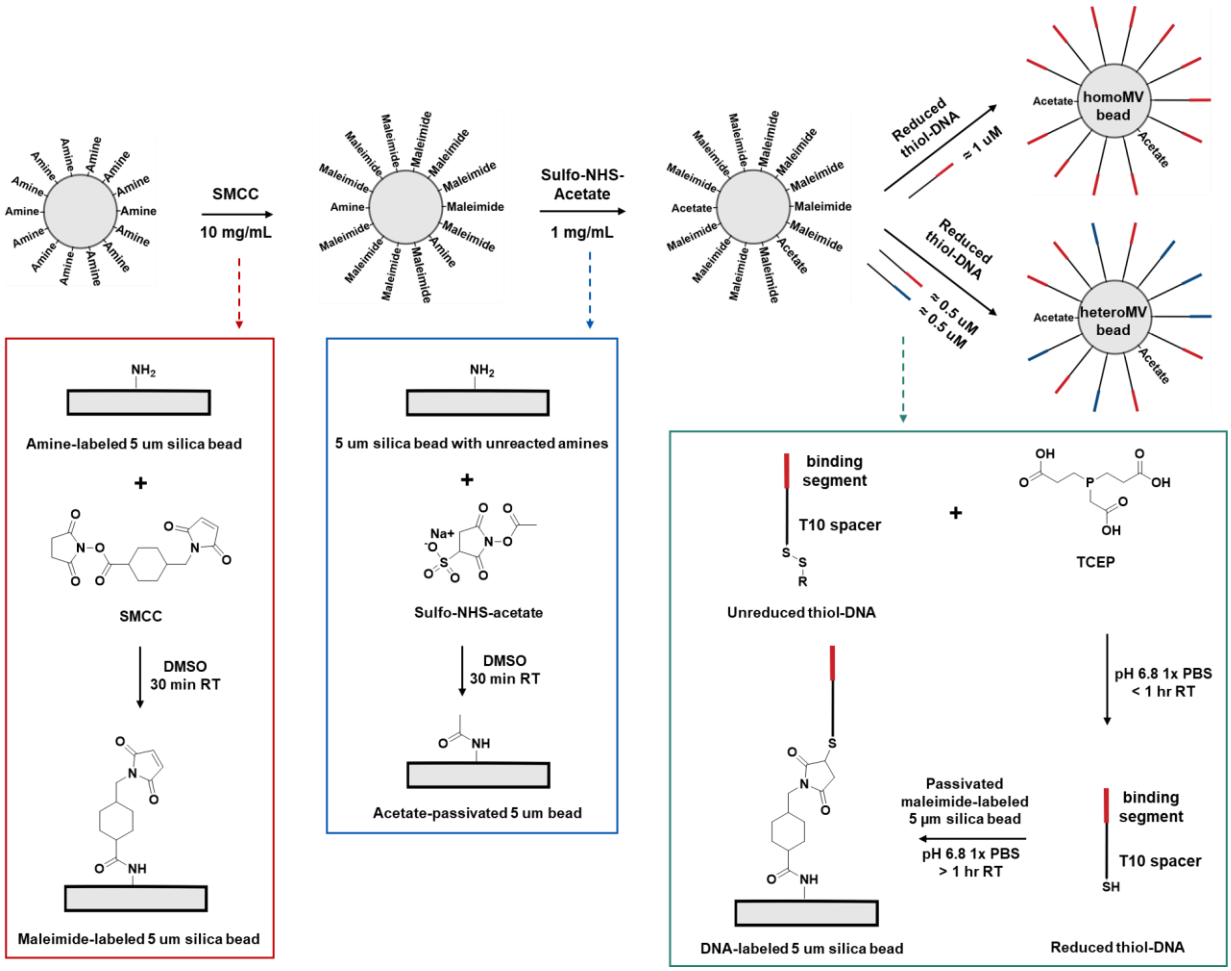

Figure S8. Characterization of DNA-functionalized silica particles.
(A) Brightfield microscopy images of 5 µm silica beads incubated in 0 M or 0.1 M KOH overnight. (B) Oligreen fluorescence intensity after incubation of 0 or 100 nM of a 20 nt oligo in 0 or 0.1 M KOH for ~6 hours. Following incubation, each sample was split into two tubes, and then Oligreen was added directly to the first tube and added following P2 gel filtration to the second tube. The plot shows that the presence of KOH in solution inhibits Oligreen fluorescence and that removing KOH using a P2 gel before adding Oligreen enables strong Oligreen fluorescence, though some DNA may be lost during filtration. (C) Flow cytometry plot showing side scatter vs forward scatter area of DNA-coated 5 µm silica beads after incubation in 0.1 M KOH for 0, 1, 4, or 8 hours. The plot shows that over time, the bead size is reduced, and the bead structure is damaged following KOH incubation, suggesting that the DNA has been released from the bead surface. (D) Oligreen fluorescence intensity following incubation of beads in 0.1 M KOH for 0, 1, 4, 8, or 24 hours, followed by P2 gel filtration. The plot indicates that all of the DNA has been released from the beads after ~8 hours. (E) Scheme showing the finalized assay for quantifying the density of the DNA on the silica beads using the Oligreen reagent. (F) Standard curves of Oligreen fluorescence intensity vs [DNA] from different concentrations of 4 different oligo mixtures. (G) Table showing the # of beads, the measured [DNA], DNA/µm^2 on the bead surface, and the calculated distance between each oligo on the bead surface. (H) Approximately-to-scale illustration of a 6R-10S bead binding the no spacer G12C target based on the DNA density measurements and literature values for single stranded and double stranded DNA lengths.

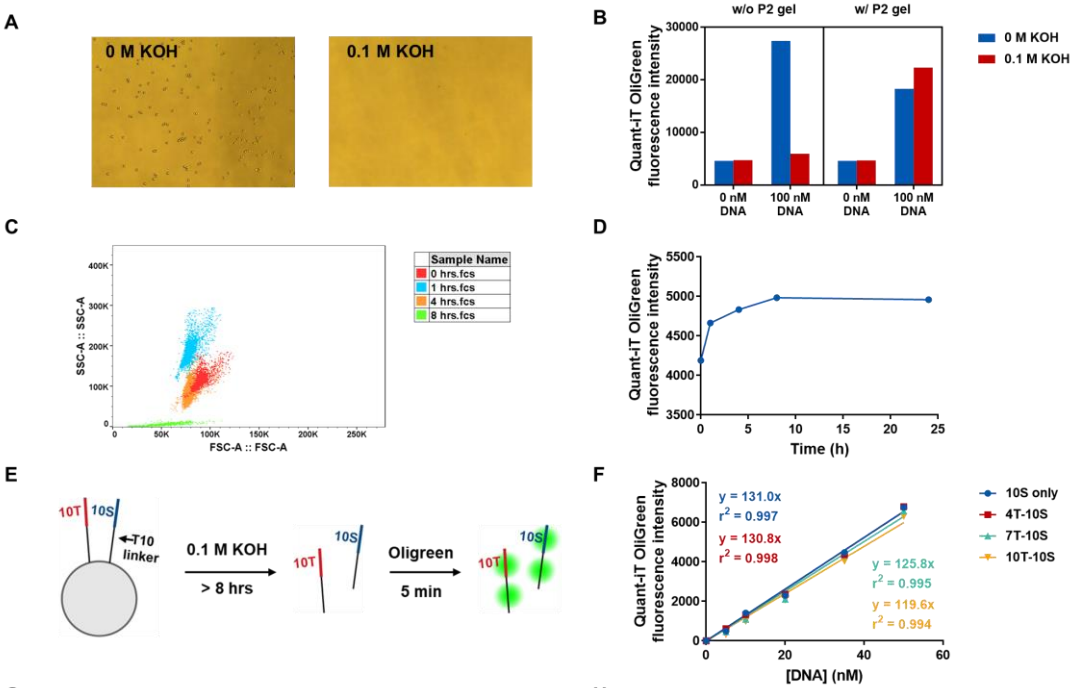

Bead name	# of beads	Total DNA concentration (nM)	DNA/um^2	distance between each oligo (nm)
10S only	9.4 x 10^4 1.6 x 10^5	4.46 8.84	3.6 x 10^4 4.1 x 10^4	5.2 4.9
4T-10S	9.0 x 10^4 1.6 x 10^5	5.55 8.88	4.7 x 10^4 4.3 x 10^4	4.6 4.8
7T-10S	1.2 x 10^5 2.0 x 10^5	6.09 8.98	4.0 x 10^4 3.4 x 10^4	5.0 5.5
10T-10S	8.7 x 10^4 1.5 x 10^5	3.76 9.89	3.3 x 10^4 5.0 x 10^4	5.5 4.5
Avg. ± SEM			4.1 ± 0.2 x 10^4	5.0 ± 0.1

Figure S9. Fluorescence microscopy images of beads hybridized to target.
Brightfield and epifluorescence microscopy images of full-length complement beads hybridized to 1 nM of Atto647N-labeled Omicron target or no target.

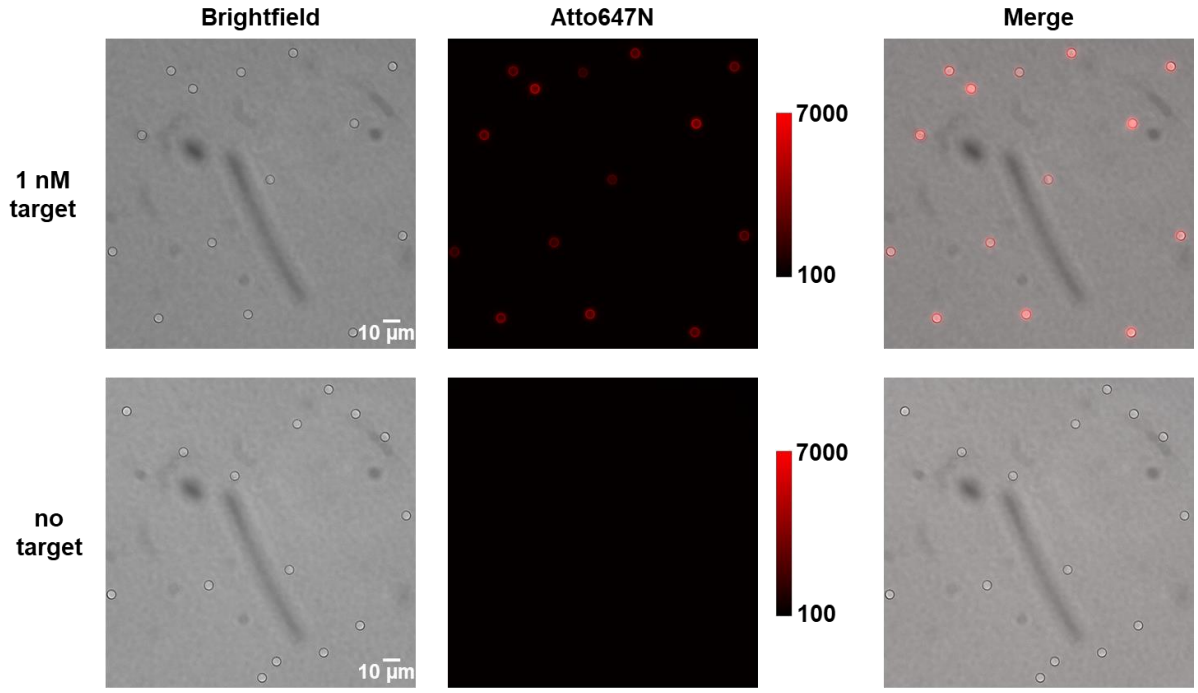

Figure S10. Flow cytometry gating strategy to isolate singlet beads for analysis.
(A) For each sample, all events are first plotted on a side scatter area vs forward scatter area plot and a “singlets area” gate is drawn to approximately include just the singlet bead population. (B) The cells included in the “singlets area” gate are then plotted on a side scatter height vs forward scatter height plot and a second gate, the “singlets height” gate, is drawn to more accurately include just the singlet bead population. The cells included in the “singlets height” gate are then used as the final singlet bead population shown in the representative histograms and from which the median fluorescence intensity values were calculated.

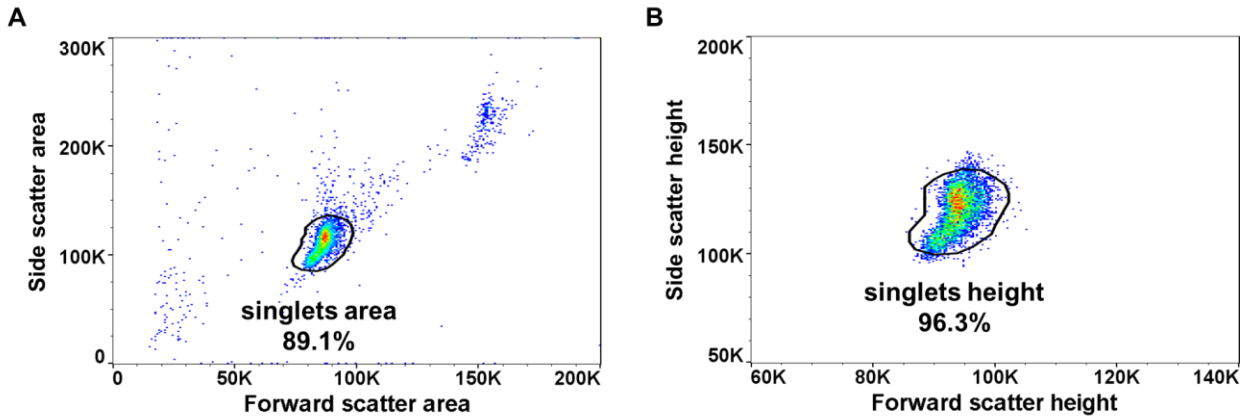

Figure S11. Representative histograms for all bead combinations binding the no spacer targets.

(A and B) Representative histograms for all bead combinations binding the no spacer G12C target (A) and WT target (B) with one plot for each heatmap column from **Figures 2C and 2D**.

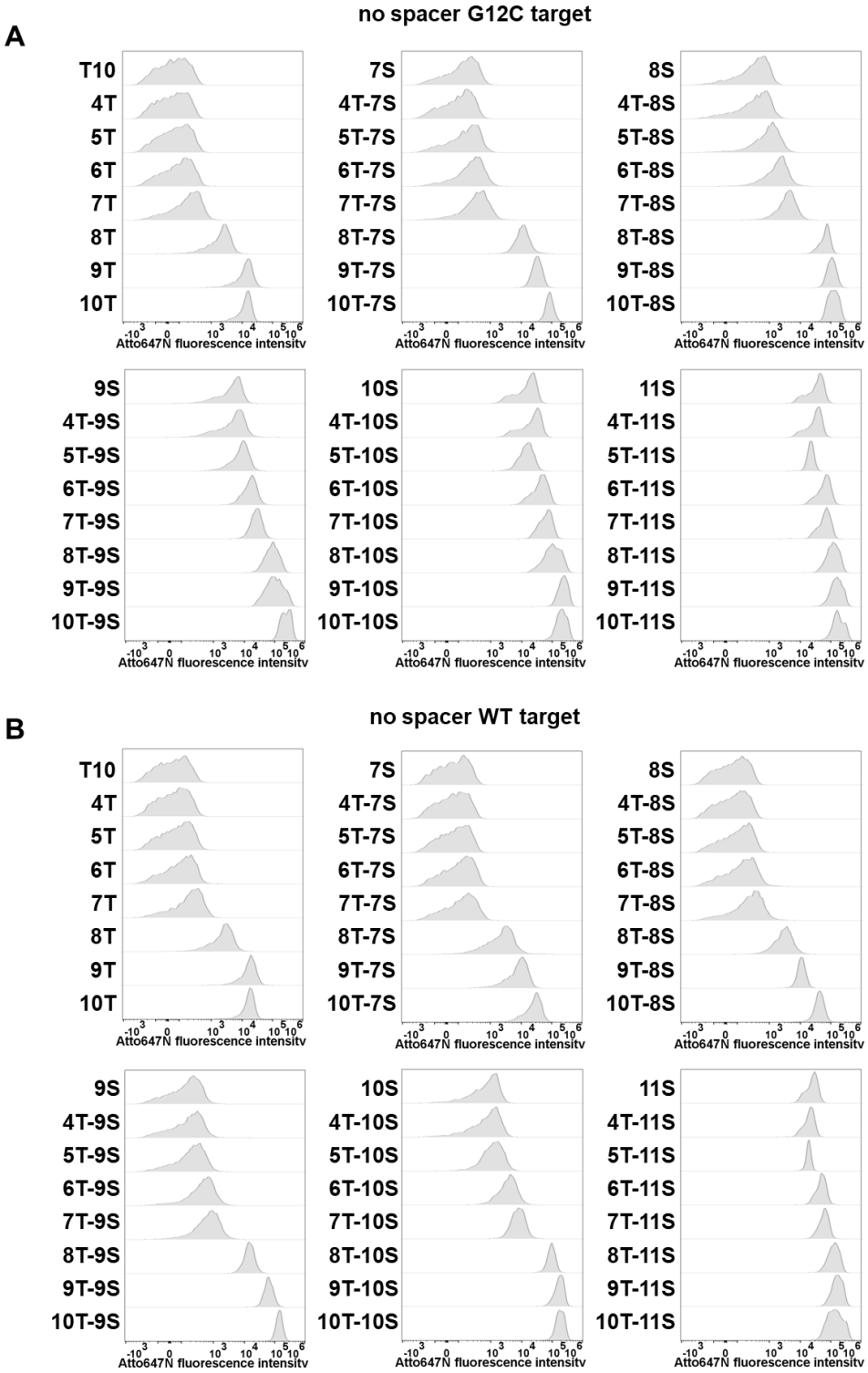

Figure S12. Impact of spacer length and type on binding of 8T, 8S, and 8T-8S beads. (A) Representative histograms for the 8T-8S beads binding the WT or G12C version of each of the different spacer length and spacer type targets. (B) Representative histograms for the 8T, 8S, and 8T-8S beads binding the G12C version of each of the different spacer length and spacer type targets. (C and D) A simplified hypothetical illustration showing the 8T (C) and 8S (D) beads binding multivalently to an internal spacer-containing target. (E and F) Scheme showing the possible base pairs formed for the 8T (E) and 8S (F) beads binding multivalently to the target. (G-J) Measured median fluorescence intensity values for the 8T (G and I) and 8S (H and J) beads binding the G12C (G and H) or WT (I and J) version of each of the different spacer length and spacer type targets. Error bars represent standard error of the mean.

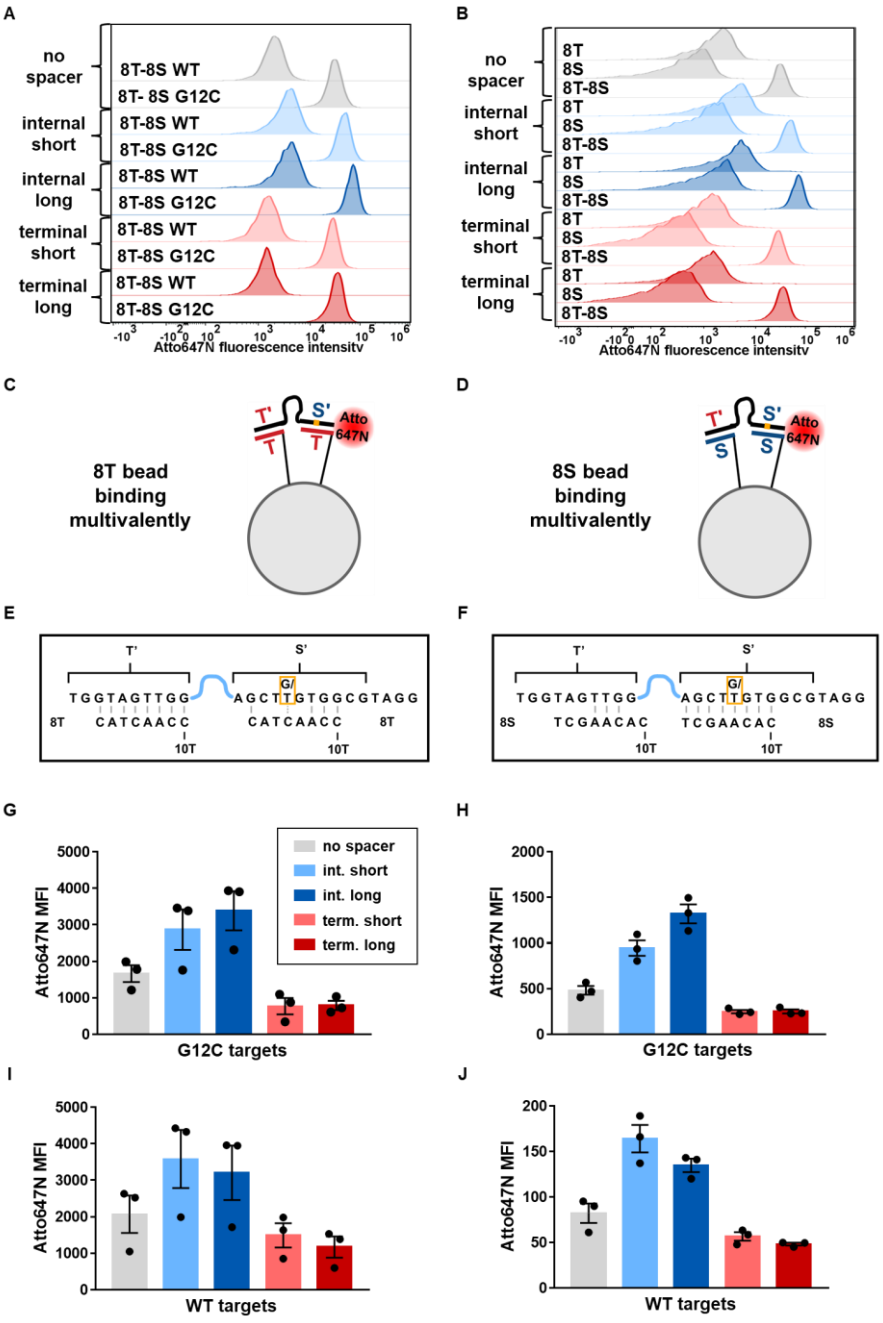

Figure S13. Impact of linker orientation on *n*=1 bead binding and representative histograms for *n*=2 beads binding WT targets.
(A) Scheme illustrating the possible binding interaction of the 5' 8T, 3' 8T, 5' 8S, and 3' 8S beads binding the no spacer G12C target monovalently. (B) Measured median fluorescence intensity values for the 5' 8T, 3' 8T, 5' 8S, and 3' 8S beads binding the no spacer G12C target. (C and D) Representative histograms (C) and measured median fluorescence intensity values (D) for 8T-8S beads with head-to-tail, head-to-head, or tail-to-tail orientation binding the WT target with no spacer, short spacer, or long spacer. (E) Representative histograms for 8T-8S beads with head-to-tail, head-to-head, or tail-to-tail orientation binding the G12C and WT no spacer targets. (F) Measured discrimination factors for 8T-8S beads with head-to-tail, head-to-head, or tail-to-tail orientation binding the no spacer, short spacer, or long spacer targets. Error bars represent standard error of the mean. Values were compared using paired one-way ANOVA with multiple comparisons follow-up tests ($^{ns}P > 0.05$, $^{*}P < 0.05$).

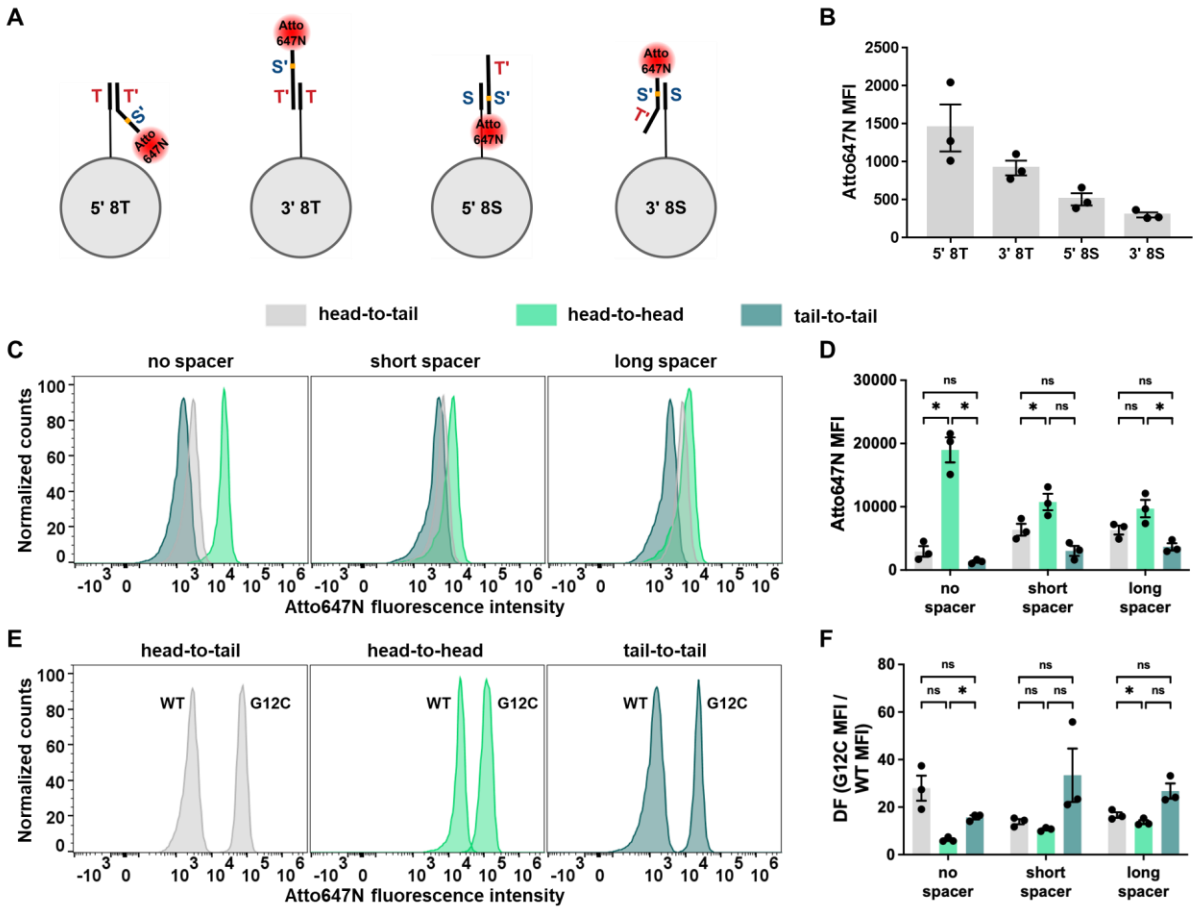

Figure S14. Representative histograms and results for all bead combinations binding the SNP_1/SNP_2, WT_1/SNP_2, SNP_1/WT_2, and WT_1/WT_2 targets.

(A and B) Scheme showing the sequences, anchor location, and spacer length for each bead combination with the head-to-tail orientation (A) or head-to-head orientation (B) and corresponding representative histograms for each bead combination binding the SNP_1/SNP_2, WT_1/SNP_2, SNP_1/WT_2, and WT_1/WT_2 targets. (C and D) Measured discrimination factors for SNP_1, SNP_2, or SNP_1 + SNP_2 for each bead combination with the head-to-tail orientation (C) or head-to-head orientation (D). Error bars represent standard error of the mean.

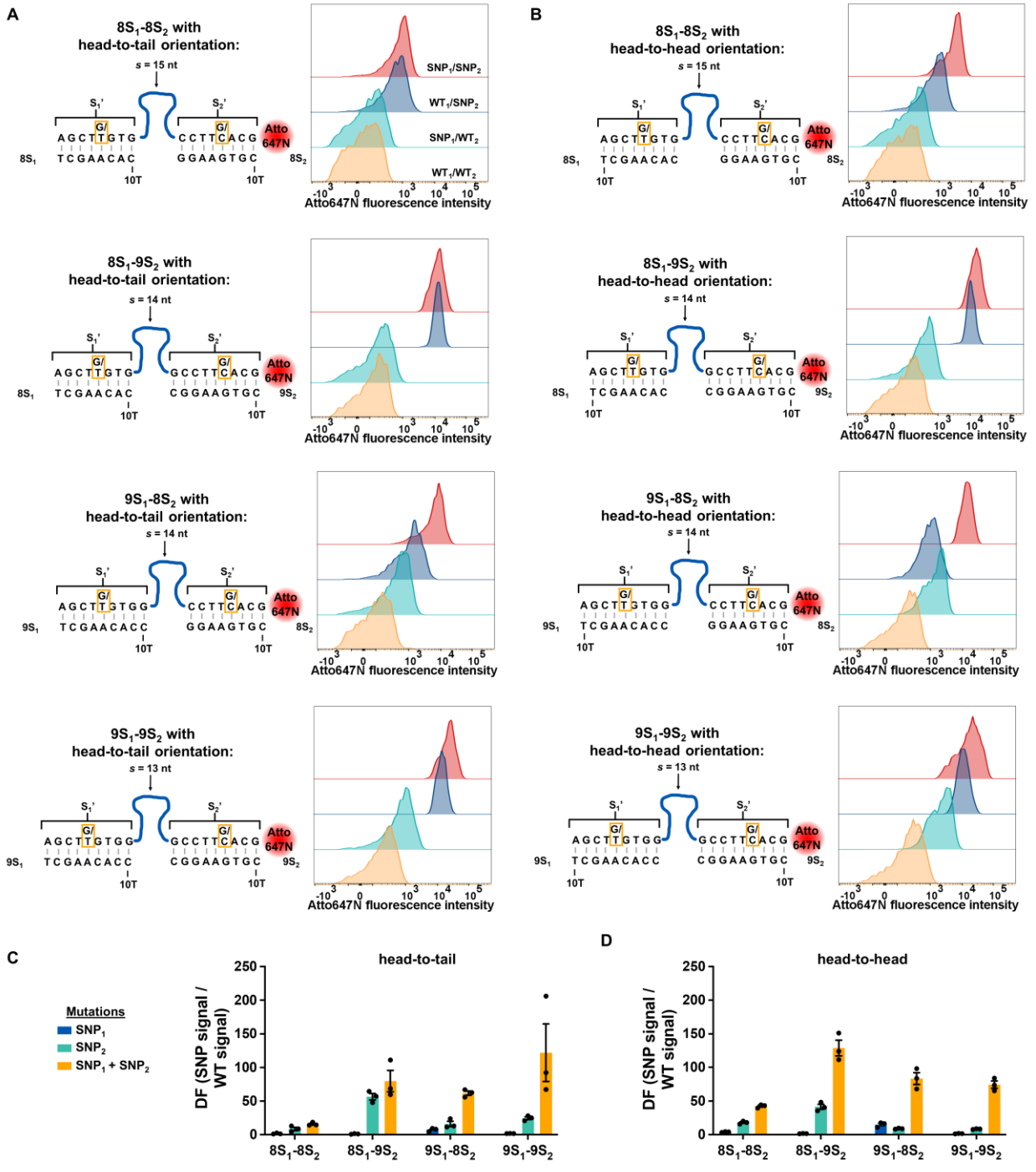

Figure S15. Representative histograms and results for all bead combinations binding the model SARS-CoV-2 targets.

(A-D) Scheme showing the sequences, anchor location, and spacer length, and corresponding representative histograms for the $8S_1$-$8S_2$ (A), $8S_1$-$9S_2$ (B), $9S_1$-$8S_2$ (C), and $9S_1$-$9S_2$ (D) beads binding the Original, Alpha, and Omicron strain targets. (E) Measured median fluorescence intensity values for each bead combination binding the three targets. (F) Measured discrimination factors for the Omicron target versus the Original or Alpha targets for each bead combination. Error bars represent standard error of the mean.

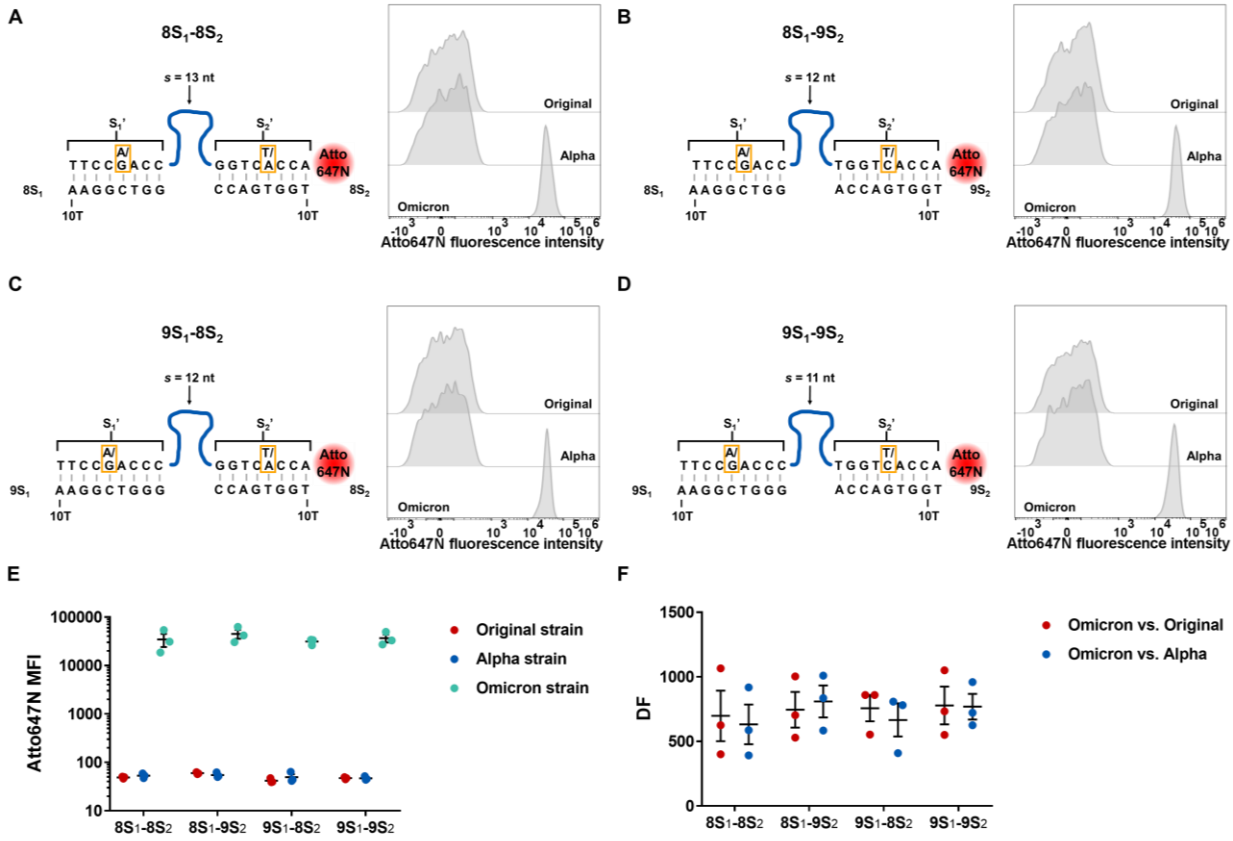

Table S1. Average median fluorescence intensity ± standard error of the mean values for all bead combinations binding no spacer G12C target.

The median fluorescence intensity of the no spacer G12C target binding to each bead combination was measured in three independent experiments. The table below shows the calculated average and standard error of the mean for the three median fluorescence intensity values.

	No S	7S	8S	9S	10S	11S
No T	59 ± 4	154 ± 13	517 ± 73	4522 ± 540	15126 ± 1789	35194 ± 935
4T	54 ± 2	120 ± 6	472 ± 33	4939 ± 328	22647 ± 423	34573 ± 1503
5T	93 ± 10	161 ± 26	1076 ± 78	8951 ± 560	14087 ± 589	40989 ± 10285
6T	106 ± 2	298 ± 19	1779 ± 89	15111 ± 396	42858 ± 1714	62873 ± 2816
7T	235 ± 13	424 ± 33	3658 ± 256	20935 ± 2115	51019 ± 5841	68290 ± 1784
8T	2369 ± 118	10610 ± 920	53619 ± 7605	81596 ± 9674	97022 ± 8979	125280 ± 4197
9T	14828 ± 1224	28731 ± 5128	76229 ± 16169	112663 ± 27240	195151 ± 22429	154005 ± 4026
10T	13744 ± 1450	81537 ± 4328	148605 ± 14991	213091 ± 9045	205227 ± 5447	176200 ± 2110

Table S2. Average median fluorescence intensity ± standard error of the mean values for all bead combinations binding no spacer WT target.

The median fluorescence intensity of the no spacer WT target binding to each bead combination was measured in three independent experiments. The table below shows the calculated average and standard error of the mean for the three median fluorescence intensity values.

	No S	7S	8S	9S	10S	11S
No T	56 ± 4	64 ± 1	72 ± 3	174 ± 12	661 ± 97	24728 ± 962
4T	61 ± 7	64 ± 3	74 ± 3	213 ± 20	909 ± 72	21385 ± 1218
5T	109 ± 10	75 ± 9	113 ± 4	251 ± 14	1225 ± 78	29084 ± 6095
6T	125 ± 1	118 ± 3	170 ± 5	475 ± 21	4040 ± 346	50386 ± 2148
7T	208 ± 19	139 ± 4	277 ± 11	647 ± 121	7234 ± 404	62561 ± 1675
8T	1955 ± 635	2262 ± 117	2826 ± 58	10898 ± 2346	81904 ± 7503	124810 ± 3137
9T	13597 ± 2110	8693 ± 1292	9635 ± 1436	60413 ± 8188	159425 ± 13751	154441 ± 13439
10T	18205 ± 1140	25845 ± 523	38530 ± 3431	130354 ± 5038	166468 ± 18349	166092 ± 14714

Table S3. Average discrimination factor ± standard error of the mean values for all bead combinations binding no spacer targets.

The median fluorescence intensity of the no spacer G12C (**Table S1**) and WT (**Table S2**) targets binding to each bead combination was measured in three independent experiments. The discrimination factor was calculated for each independent replicate by dividing the G12C MFI value by the WT MFI value. The table below shows the calculated average and standard error of the mean for the three discrimination factor values.

	No S	7S	8S	9S	10S	11S
No T	1.0 ± 0.0	2.4 ± 0.2	7.2 ± 0.8	25.9 ± 1.4	23.2 ± 2.0	1.4 ± 0.1
4T	0.9 ± 0.1	1.9 ± 0.1	6.4 ± 0.3	23.3 ± 0.6	25.2 ± 2.0	1.6 ± 0.0
5T	0.8 ± 0.0	2.1 ± 0.2	9.5 ± 0.7	35.6 ± 1.4	11.5 ± 0.3	1.4 ± 0.1
6T	0.8 ± 0.0	2.5 ± 0.2	10.5 ± 0.8	31.8 ± 0.6	10.7 ± 0.5	1.2 ± 0.0
7T	1.2 ± 0.1	3.1 ± 0.3	13.2 ± 0.6	33.9 ± 4.4	7.1 ± 0.8	1.1 ± 0.0
8T	1.8 ± 1.0	4.7 ± 0.2	18.9 ± 2.3	8.0 ± 1.3	1.2 ± 0.2	1.0 ± 0.0
9T	1.1 ± 0.2	3.3 ± 0.3	7.9 ± 1.1	1.8 ± 0.2	1.2 ± 0.1	1.0 ± 0.1
10T	0.8 ± 0.0	3.2 ± 0.2	3.9 ± 0.6	1.6 ± 0.0	1.3 ± 0.1	1.1 ± 0.1

Table S4. Average cooperativity factor ± standard error of the mean values for all bead combinations binding no spacer G12C target.

The median fluorescence intensity of the no spacer G12C (**Table S1**) target binding to each bead combination was measured in three independent experiments. The average cooperativity factor was calculated by dividing the average *n*=2 MFI by the average of the average corresponding *n*=1 MFIs. The standard error of the mean was calculated by propagating the SEMs from the three independent MFI measurements for the *n*=2 beads and the *n*=1 beads. The table below shows the calculated average cooperativity factor and standard error of the mean.

	7S	8S	9S	10S	11S
4T	1.2 ± 0.1	1.7 ± 0.2	2.2 ± 0.3	3.0 ± 0.4	2.0 ± 0.1
5T	1.3 ± 0.2	3.5 ± 0.5	3.9 ± 0.5	1.9 ± 0.2	2.3 ± 0.6
6T	2.3 ± 0.2	5.7 ± 0.7	6.5 ± 0.8	5.6 ± 0.7	3.6 ± 0.2
7T	2.2 ± 0.2	9.7 ± 1.2	8.8 ± 1.3	6.6 ± 1.1	3.9 ± 0.1
8T	8.4 ± 0.8	37.2 ± 5.6	23.7 ± 3.4	11.1 ± 1.5	6.7 ± 0.3
9T	3.8 ± 0.8	9.9 ± 2.3	11.6 ± 2.9	13.0 ± 1.8	6.2 ± 0.2
10T	11.7 ± 1.4	20.8 ± 3.0	23.3 ± 2.2	14.2 ± 1.2	7.2 ± 0.3

Supporting References

1. Hail, M.; Elliott, B.; Anderson, K., High Throughput Analysis of Oligonucleotides Using Automated Electrospray Ionization Mass Spectrometry. *Am Biotechnol Lab* **2004,** *12*, 12-14.